






Article

Investigating the Potential Climatic Effects of Atmospheric Pollution across China under the National Clean Air Action Plan

Adil Dilawar ^{1,2} , Baozhang Chen ^{1,2,3,*} , Zia Ul-Haq ⁴, Muhammad Amir ^{2,5} , Arfan Arshad ⁶ , Mujtaba Hassan ⁷, Man Guo ⁸, Muhammad Shafeeqe ⁹ , Junjun Fang ^{1,2}, Boyang Song ¹⁰ and Huifang Zhang ^{1,2}

- ¹ State Key Laboratory of Resources and Environmental Information System, Institute of Geographic Sciences and Natural Resources Research, Chinese Academy of Sciences, Beijing 100101, China
- ² University of Chinese Academy of Sciences (UCAS), Beijing 100049, China
- ³ Jiangsu Center for Collaborative Innovation in Geographical Information Resources Development and Application, Nanjing 210023, China
- ⁴ Remote Sensing, GIS and Climatic Research Lab, National Center of GIS and Space Applications, Centre for Remote Sensing, University of the Punjab, Lahore 54590, Pakistan
- ⁵ Key Laboratory of Ecosystem Network Observation and Modeling, Institute of Geographic Sciences and Natural Resources Research, Chinese Academy of Sciences, Beijing 100101, China
- ⁶ Department of Biosystems and Agricultural Engineering, Oklahoma State University, Stillwater, OK 74078, USA
- ⁷ Department of Space Science, Institute of Space Technology, Islamabad 44000, Pakistan
- ⁸ School of Geographical Sciences, Faculty of Science and Engineering, University of Nottingham, Ningbo 315100, China
- ⁹ Climate Lab, Institute of Geography, University of Bremen, 28359 Bremen, Germany
- ¹⁰ School of Remote Sensing and Geomatics Engineering, Nanjing University of Information Science and Technology, Nanjing 210044, China
- * Correspondence: baozhang.chen@igsrr.ac.cn



Citation: Dilawar, A.; Chen, B.; Ul-Haq, Z.; Amir, M.; Arshad, A.; Hassan, M.; Guo, M.; Shafeeqe, M.; Fang, J.; Song, B.; et al. Investigating the Potential Climatic Effects of Atmospheric Pollution across China under the National Clean Air Action Plan. *Remote Sens.* **2023**, *15*, 2084. <https://doi.org/10.3390/rs15082084>

Academic Editors: Sonoyo Mukai and Adrianos Retalis

Received: 28 February 2023

Revised: 11 April 2023

Accepted: 11 April 2023

Published: 14 April 2023



Copyright: © 2023 by the authors. Licensee MDPI, Basel, Switzerland. This article is an open access article distributed under the terms and conditions of the Creative Commons Attribution (CC BY) license (<https://creativecommons.org/licenses/by/4.0/>).

Abstract: To reduce air pollution, China adopted rigorous control mechanisms and announced the Air Pollution Prevention and Control Action Plan (APPCAP) in 2013. Here, using OMI satellite, the NASA Socioeconomic Data and Application Center (SEDAC), and Fifth ECMWF (ERA5) data at a $0.25^\circ \times 0.25^\circ$ resolution, we explored changes in NO_2 , PM, SO_2 , and O_3 and climatology over China in response to the Action Plan between 2004 and 2021. This study attempts to investigate the long term trend analysis of air pollution and climatic variations during two scenarios before (2004–2013) and after (2013–2021) APPCAP. We investigated the climatic effects of air pollution in China before and after APPCAP adoption using geographically weighted regression (GWR) and differential models to assess the contribution of air pollution. The spatial representation analysis demonstrated how air pollution affected climatic factors before and after the APPCAP. Several important findings were derived: (1) the APPCAP significantly influenced air pollution reduction in China post-scenario (2013–2021); (2) the Mann Kendall test investigated that all pollutants showed an increasing trend pre-APPCAP, while they showed a decreasing trend, except for O_3 , post-APPCAP; (3) for climatic factors, the MK test showed an increasing trend of precipitation and mean minimum air temperature t_{\min} post-APPCAP; (4) innovative trend analysis (ITA) showed a reduction in NO_2 , SO_2 , and PM, although O_3 showed no trend post-APPCAP; and (5) pre-scenario, NO_2 contributed to an increase in the mean maximum air temperature (t_{\max}) by 0.62°C , PM contributed to raising t_{\min} by 0.41°C , while O_3 reduced the $t_{\max}(t_{\min})$ by 0.15°C (0.05°C). PM increased t_{\max} and precipitation with a magnitude 0.38°C (7.38 mm), and NO_2 contributed to increasing t_{\min} by (0.35°C), respectively, post-scenario. In particular, post-scenario led to an increase in t_{\min} and precipitation across China. The results and discussion presented in this study can be beneficial for policymakers in China to establish long-term management plans for air pollution and climatological changes.

Keywords: air pollution; APPCAP; Geographically weighted regression (GWR); meteorology

1. Introduction

Climatic change is a worldwide phenomenon that has become more obvious in the last three decades [1,2]. As a global phenomenon, there has been an increasing interest in examining the effects of climatic changes. According to the Fifth Assessment Report from the Intergovernmental Panel on Climate Change (IPCC), global land and ocean temperatures increased by 0.85 °C during 1880–2012 [3,4]. GHGs, aerosols, and change of land use patterns due to anthropogenic activities have altered the Earth's radiative balance and albedo [5–8]. Alterations in the Earth's radiative balance, through complex mechanisms, are responsible for changes in temperature, precipitation, and other climatic variables. Furthermore, significant climate crises can be attributed to the key drivers of climate variations, which include solar irradiance and volcanic eruptions [9,10]. Solar irradiance serves as the Earth's primary energy source, directly impacting the climate system by influencing ozone concentrations, which induce substantial changes in atmospheric heating and circulation [11–13]. Volcanic eruptions are the most powerful natural phenomena of the industrial era, with minor eruptions occurring worldwide and emitting particles that remain confined in the troposphere for several weeks. On the other hand, explosive eruptions emit a significant amount of ash and SO₂ into the stratosphere, causing short-term climatic effects [14,15]. Urbanization has modified the local climate through the intensification of urban heat island (UHI) intensity effects, with UHI intensity continuously increasing, particularly in megacities [16–19].

Environmental pollution has affected the ecosystem and climate directly and indirectly, resulting in economic and social costs [20–22]. Air pollution is a prime global concern due to human activities and severe meteorological conditions [23–25]. Multiple studies have investigated the effects of air pollution impacts on human health, demonstrating reduced life expectancy and well-being, particularly in urban and industrialized areas [26–29]. The public awareness of environmental pollution and its challenges varies across the globe, with different stages of industrialization and urbanization in different countries. During the initial stages of industrialization, local economies were boosted, it raised prosperity, and people were less concerned with the negative effects of environmental pollution on the ecosystem [30,31]. China's rapid economic expansion has led to significant pollution emissions and environmental devastation, with detrimental impacts on the local and regional environment [32,33]. Climatic change and air pollution are intrinsically linked, as air pollutants such as NO₂, PM, SO₂, and O₃ interact with solar and terrestrial radiation, contributing to climate perturbations [34,35]. SO₂, in particular, is a significant pollutant that causes severe health risks to individuals and environmental deterioration [36]. Changes in different atmospheric pollutants induce radiative forcing (RF), which perturbs the atmospheric and climate system [37].

In the context of climatic change, air pollutants disturb the amount of incoming sunlight that is absorbed or reflected by the atmosphere, resulting in significant impacts on the climate. Anthropogenic emissions cause adverse meteorological conditions [38,39]. Some studies have explored the systematic relationship between air pollution and climatic variables [40,41]. Moreover, air pollutants alter surface climates, including precipitation and temperature patterns [42]. Ramanathan (2005) and Sillmann (2017) investigated how aerosols could impact precipitation patterns and concluded that air pollution significantly alters precipitation patterns, including the monsoon cycle worldwide [43–46]. Over the last three decades, countries in Asia, such as China, India, Pakistan, and Nepal, have experienced severe air pollution because of industrialization and urbanization. The history of air pollution control shows that only increased awareness about the adverse impacts of pollution on health makes the governments take strict control measures [47,48]. Global industrialization, including in China today, has degraded ecosystems [49], depleted natural resources, and has had adverse effects on ozone levels that may harm plants and impair human health [30,50,51].

Due to the spatial scarcity of the consistent distribution of site stations, accurately assessing air pollution and the distribution of meteorological factors and their relationships

becomes challenging. Under such conditions, satellite and reanalysis data provide a significant opportunity to assess these phenomena. Many studies have explored the long-term variation of air pollutants and their interaction with climatic factors using ozone monitoring instrument (OMI) satellite data [52,53]. OMIs have been used for a variety of studies, such as analyzing the relationship between air pollutants (NO_2 , O_3 , SO_2 , CO) and meteorological factors over Bangladesh [54], analyzing the trends in NO_2 and SO_2 [55–58], evaluating the pollution emission inventory [59], as well as analyzing the long-term trends of NO_2 and SO_2 over East China [60]. Reanalysis datasets are potential alternatives for studying climate variability [61]. NASA SEDAC has provided high resolution PM data to analyze trends and impacts [62–64]. The ERA-interim and its new version, ERA5, are global reanalysis data made by the European Center for Medium Range Weather Forecasts (ECMWF). These reanalysis datasets include many climate state variables and provide ideal data for investigating climatic changes and improving water resource policies [65]. The hydrological regime of the Gilgit Basin in Pakistan was studied using ERA5 [66].

In response to heavy pollution and related concerns, the Chinese government has adopted certain measures to improve air quality and reduce environmental pollution [67]. China's State Council has adopted three major action plans to control air, water, and soil pollution. In comparison to water and soil pollution, air pollution has gained more attention because it has significant spatial impacts and is highly visible [68,69]. To improve air quality in China, on 12 September 2013, the China State Council issued an action plan named APPCAP to guide the national efforts to prevent and reduce air pollution [70]. This action plan demanded a reduction in the mean annual concentrations of $\text{PM}_{2.5}$ between 15% and 25% across key regions. In this regard, the Chinese government has had the goal of reducing emissions of $\text{PM}_{2.5}$ and other pollutants since 2012 [71,72]. In 2013, the National Environmental Monitoring Center (NEMC) and the National Ministry of Environmental Protection (MEP) started monitoring public hourly and daily air quality data. As a consequence of the Chinese government's enforcement of policies and measures, some types of pollution have been reduced over the last decade, such as smog, haze, and acid deposition [73–75]. By adopting the clean air action plan in 2013, China has achieved an average yearly reduction of 4.9%, 12.0%, and 5.3% for NO_2 , SO_2 , and CO , respectively, during 2014–2015. These reductions are considered to make APPCAP the most promising air pollution combat policy in China to date to improve air quality. To understand the promising efforts of China, the current research divided the study period into two different scenarios: before APPCAP (pre-scenario) and after APPCAP (post-scenario). The APPCAP is a milestone in air pollution control efforts in China and encourages researchers to evaluate the effect of air pollution management and its impacts at the national level in China. However, there is still lack of a methodology framework to investigate the air pollution association with the regional climatic variables under the context of air pollution control management in China. The current study analyzed the role of air pollution during the pre and post-scenarios based on APPCAP in regional meteorology changes (t_{\max} , t_{\min} , and precipitation) and associated impacts over China, with important implications for future air quality strategies in China. The climatic impacts of air pollution vary by location, and the air pollution-driven changes can be comparable to, or even more significant than, those caused by anthropogenic emissions [76]. Therefore, it is of great importance to identify the most influential air pollutant (NO_2 , PM , SO_2 , and O_3) for t_{\max} , t_{\min} , and precipitation changes over the whole of China since clean air actions were adopted.

This study aimed to gauge the effectiveness of the APPCAP policy in China and provide benchmarks and measurable implications for achieving air pollution mitigation strategies. To fully understand the air pollution phenomenon and apply the policy adequately, it would be helpful to clarify the aforementioned challenges, as shown in Figure 1. The current study comprehensively estimated the climatic impact of the APPCAP from 2004 to 2021 in China by following these objectives:

1. To identify the long-term variability of air pollutants (NO_2 , PM, SO_2 , and O_3) under the pre-scenario and post-scenario scheme to evaluate the comprehensive goal of APPCAP;
2. To determine the long-term trend of climatic factors (t_{\max} , t_{\min} , and precipitation) in compliance with the pollution control policy;
3. To evaluate the spatial climatic contribution of air pollution control management over the past two decades at the national level in China.

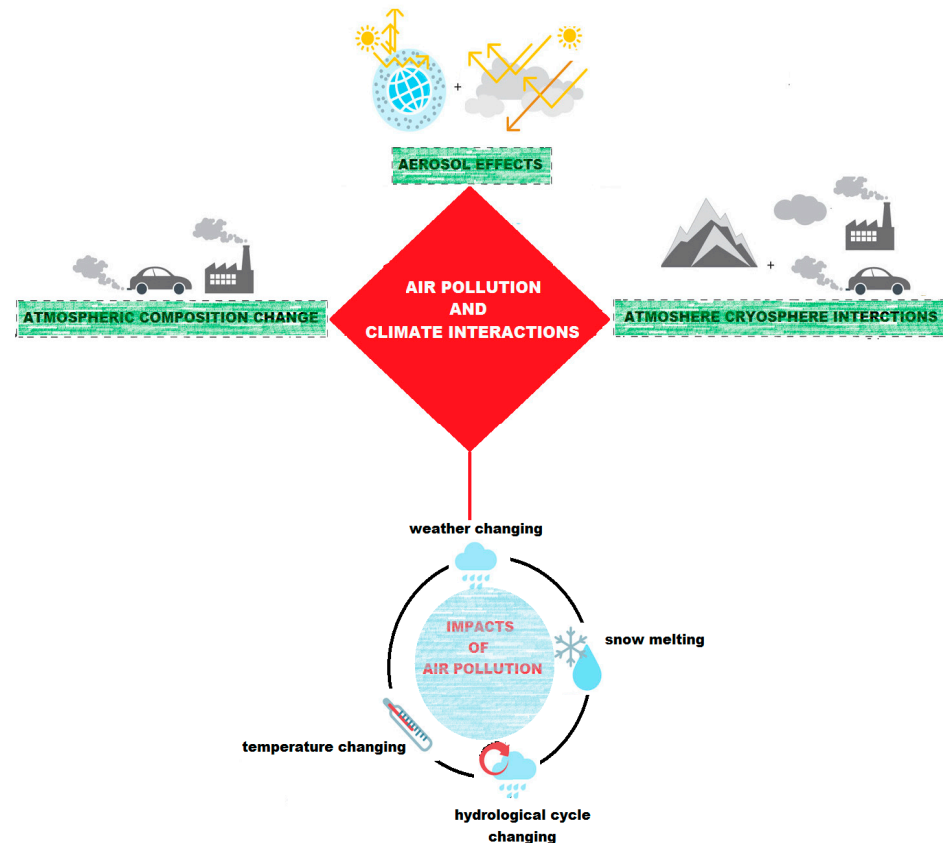


Figure 1. Flowchart diagram of air pollution interaction and impacts.

2. Materials and Methods

2.1. Study Area

China is a vast and diverse country located in East Asia, covering an area of approximately 9.6 million square kilometers. It has a population of over 1.4 billion people, making it the most populous country in the world. China is divided into six major climate regions, including the tropical, subtropical, warm, middle temperate, cold, and plateau zones [77]. The subtropical zone covers the largest area of China, while the northern part of the country experiences year-round ice and snow. The eastern and southern regions of China are influenced by the Pacific Ocean and are characterized by monsoon climates such as hot, subtropical, and temperate monsoons [78]. These zones are further divided into sub regions based on Figure 2, which shows the location of these different climate zones, providing a useful reference for studying the climate and its impact on different aspects of life in China. Air pollution is a major issue in China, with many cities experiencing high levels of PM, SO_2 , NO_2 , and O_3 . Rapid industrialization, urbanization, and the extensive use of fossil fuels have greatly contributed to China's severe air pollution problem.

The northern parts of China, including Inner Mongolia and Xinjiang, experience a continental climate, with very cold winters and hot summers. The western region of China, such as Tibet and the Himalayas, has a plateau climate, characterized by low air pressure, thin air, and a large daily temperature range. The eastern and southern regions of China

are influenced by the Pacific Ocean, with the monsoon climate dominating the area. The mountainous areas of China have a temperate climate, with cooler temperatures and lower humidity than other areas at the same altitude.

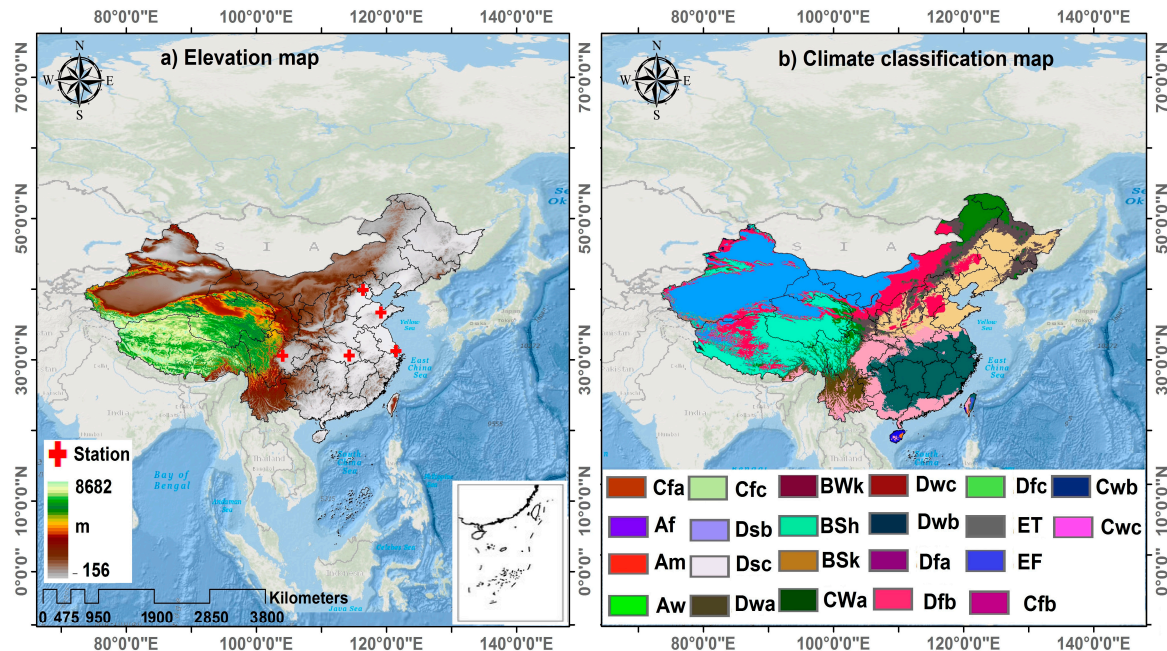


Figure 2. Study area description: (a) elevation map and (b) description of climate zones—Geiger classification in China. Main climates A: equatorial B: arid C: warm temperate D: snow E: polar Precipitation W: desert S: steppe f: fully humid s: summer dry w: winter dry m: monsoonal Temperature a: hot summer b: warm summer c: cool summer d: extremely continental h: hot arid k: cold arid F: polar frost T: polar tundra).

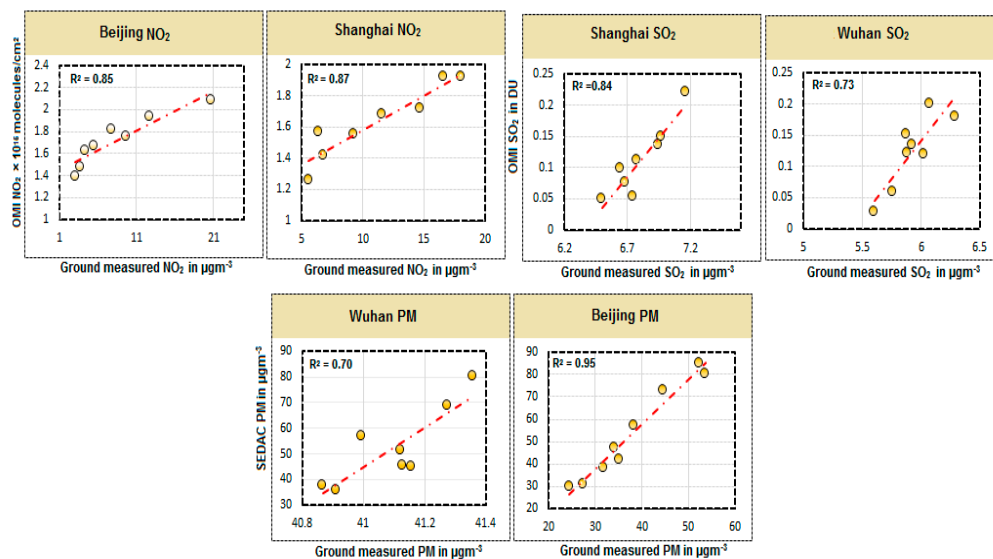
2.2. Data Description

Aura and Terra satellite-based OMI (<https://giovanni.gsfc.nasa.gov/>, accessed on 12 September 2022) measured the data of three air pollutants, including NO₂, SO₂, and O₃ [79–81]. PM data were collected from the NASA SEDAC, which provided global annual PM grids from MODIS, MISR, and SeaWiFS aerosol optical depth, v4.03 [62]. Aerosol optical depth retrievals from multiple satellite algorithms were calibrated based on Aerosol Robotic Network (AERONET) observations (<https://sedac.ciesin.columbia.edu> (10 September 2022)) [63,64]. Three meteorological parameters (temperature maximum, temperature minimum, and precipitation) were obtained from the Fifth generation (ERA5) (<https://www.ecmwf.int/en>, accessed on 28 September 2022) [82–84] as in the description written for Table 1. Ground measurements were used to compare the satellite-estimated and NASA SEDAC data at some pollution monitoring stations as different locations as indicated in Figure 1. The ground measurements for air pollutants were accessed from a website (<http://www.aqistudy.cn/>, accessed on 20 February 2023) under the control of the Ministry of Ecology and Environment, China available from 2013.

Only NO₂, PM, and SO₂ ground concentrations were used to compare the satellite measurements and NASA SEDAC PM, and a high correlation was found between them, as shown in Figure 3.

Table 1. Detailed information on data used in the current study. Note: ** Data were averaged into annual values.

Data Source	Parameter	Units	Spatial Resolution	Temporal Resolution
Ozone Monitoring Instrument (OMI) + NASA SEDAC	Nitrogen dioxide (NO ₂)	Molecules/cm ²	0.25° × 0.25°	Daily **
	Ozone (O ₃)	Dobson Units (DU)	0.25° × 0.25°	Daily **
	Sulfur dioxide (SO ₂)	Dobson Units (DU)	0.25° × 0.25°	Daily **
	Particulate Matter (PM)	µgm ⁻³	0.25° × 0.25°	Annual
Fifth-generation ECMWF (ERA5)	Temperature (max)	°C	0.25° × 0.25°	Monthly **
	Temperature (min)	°C	0.25° × 0.25°	Monthly **
	Precipitation	mm	0.25° × 0.25°	Monthly **

**Figure 3.** A comparison of the mean annual OMI measured column densities and NASA SEDAC PM with ground measured pollutants.

2.3. Trend Analysis

In the present study, we used two non-parametric statistical approaches to determine whether the meteorological and air pollutants time series were increasing, decreasing, or showing no trend. ITA and MK tests were employed to identify trends in these variables. In particular, the ITA test was used to signify efforts to control air pollution in China. Traditional monotonic trend approaches detect trends using statistical calculations and cannot depict trends in different subcategories of data values. The ITA is an intuitive method for identifying trends in different time series subcategories, regardless of distribution assumptions [85–87]. Meanwhile, the MK test assumes that time series have no sequential correlation and is based on the assumption that all data are significant [88]. These techniques are widely used to analyze climatic parameters in particular [82,89].

2.3.1. ITA Trend Analysis

The ITA approach detects disparities in air pollution data time series using a non-parametric approach. Using ITA, the time series is divided into equal halves, and each subseries is sorted in ascending order separately. The first subseries is positioned ($X_i; i = 1, 2, \dots, n/2$) on the x-axis, and the second subseries is positioned ($X_j; j = 1, 2, \dots, n/2$) on the y-axis based on the Cartesian coordinate system. Both axes must have the same range to interpret the changed information. This approach provides a quick visual understanding of the nature of time series trends. The data values lie on a 1:1 (45°) straight line, indicating that the time series has no trend. The data points that lie above or below the area of triangulation show the increasing or decreasing trends of the time series, respectively [90,91]. The first

half of the data points determines the trend change, and the trend indicator is determined by the difference between the two subseries divided by the mean of the first subseries [92].

The longitudinal trend is computed by taking the arithmetic average of the X_j and X_i values at every point in the time series. The vertical and horizontal distance from the linear line is used to calculate the absolute difference. The indicator of the trend [88,91] is computed using the following Equation (1):

$$S = \frac{2(\bar{X}_j - \bar{X}_i)}{n} \quad (1)$$

where “ S ” shows the indicator of the trend, and n is the number of data points at \bar{X}_j and \bar{X}_i , represented as the second and first subseries arithmetic averages, respectively. The positive and negative values of “ S ” show an increasing and decreasing trend. If the value of observation data is found odd in the original time series, the first observation might be discarded.

The significance of the slope was tested by the method proposed by Sen, and a description of the method was shown in [89].

Confidence limits (CLs) define the significance of the slope of the time series such as if the data points fall out of the CL, then it is statistically significant. To compute the CLs of the slope, it follows a Gaussian probability density function with zero mean and standard deviation as given below:

$$CL_{(1-\alpha)} = 0 \pm s_{cri} \times \sigma_s \quad (2)$$

where α is the significance level at a 5% confidence that was used to evaluate the significance of the ITA trend, and s_{cri} is the standard normal PDF; the value of “ s_{cri} ” can be calculated using the following equations:

$$s_{cri} = \frac{Z - \alpha}{2} \quad (3)$$

where $\alpha = 1$ for confidence level. For example, if we have a 95% confidence level, then the corresponding level of alpha is as follows:

$$\alpha = 1 - 0.95 = 0.05 \quad (4)$$

where σ_s is defined as:

$$\sigma_s = \frac{2\sqrt{2}}{n\sqrt{n}} \sigma \sqrt{1 - \rho_{\bar{x}_i, \bar{x}_j}} \quad (5)$$

where $\rho_{\bar{x}_i, \bar{x}_j}$ is the correlation coefficient between the two mean values.

$$\rho_{\bar{x}_i, \bar{x}_j} = \frac{E(\bar{X}_i \bar{X}_j) - E(\bar{X}_i) E(\bar{X}_j)}{\sigma_{\bar{x}_i} \sigma_{\bar{x}_j}} \quad (6)$$

2.3.2. Mann Kendall Trend Analysis

The aforementioned air pollution and meteorological data were evaluated to detect the spatial-temporal variation over the China region using two methods: a non-parametric MK test and Sen’s slope. The negative and positive magnitudes of trends were calculated to find the slope value and detect the trend changes in air pollution and meteorological factors in China. The MK test was used for the inhomogeneous time series data to illustrate the spatial and temporal patterns, and the ZMK test statistic was used [93,94]. The following mathematical equations were used to calculate the MK statistics $V(S)$, S , and standardized test statistic Z :

$$S = \sum_{i=1}^{n-1} \cdot \sum_{j=i+1}^n \text{sign}(X_j - X_i),$$

$$\text{sign}(X_j - X_i) = \begin{cases} +1 & \text{if } (X_j - X_i) > 0 \\ 0 & \text{if } (X_j - X_i) = 0 \\ -1 & \text{if } (X_j - X_i) < 0, \end{cases}$$

$$V(S) = \left[n(n-1)(2n+5) - \sum_{p=1}^q t_p(t_p-1)(2t_p+5) \right],$$

$$Z = \begin{cases} \frac{S-1}{\sqrt{\text{VAR}(S)}} & \text{if } S > 0 \\ 0 & \text{if } S = 0 \\ \frac{S-1}{\sqrt{\text{VAR}(S)}} & \text{if } S < 0, \end{cases} \quad (7)$$

n is length of time, t_p is the tied values for the p th value, and q is the number of tied values, while X_i and X_j are the data values in chronological order. In the current study, the significance of the trend was tested at the Z -critical value > 1.96 with a significance level of 0.05. The null hypothesis of no trend must satisfy the condition if $-1.96 > ZMK > 1.96$.

2.4. Geographically Weighted Regression Model (GWR)

The GWR model was extensively used in this study to investigate the relationship between the climatic parameters and air pollutants at the national scale of China. GWR modeling is a type of regression modeling with geographically varying parameters (e.g., air pollutants), which differs from conventional regression modeling and was developed to achieve a higher performance in geographical analysis. In general, the GWR model can be expressed by the following Equations (8) and (9) [54,95]:

$$C_i = \sum_k \beta_k(X_i Y_i) AP_{k,i} + \varepsilon_i \quad (8)$$

where C_i is the spatial dependent variable at the location i ; $X_i Y_i$ is the x - y coordinate of the i_{th} location. $\beta_k(X_i Y_i)$ is the coefficient, a varying conditional at k_{th} , and the respective x - y location with the first coefficient by setting $AP_{0,i} = 1$, that is $\beta_0(X_i Y_i)$ defined as the geographically varying intercept term. $AP_{k,i}$ is the independent variable at k_{th} and the respective x - y location. ε_i is the Gaussian error at the x - y coordinate of the i_{th} location:

$$C_i = \beta_0(X_i, Y_i) + \beta_1(X_i, Y_i) NO_2 + \beta_2(X_i, Y_i) PM + \beta_3(X_i, Y_i) SO_2 + \beta_4(X_i, Y_i) O_3 + \varepsilon_i \quad (9)$$

where C_i stands for the dependent climatic factors (precipitation, temperature maximum, and temperature minimum). $\beta_0(X_i, Y_i)$ is the geographical intercept. β_1 to $\beta_4(X_i, Y_i)$ are the respective geographically varying coefficients, which are different from the coefficients of conventional regression. NO_2 , PM , SO_2 , and O_3 are the independent air pollutants at the x - y coordinate of the i_{th} location.

2.5. Impact Assessment of Air Pollution on Climate

The climatic impact of air pollution can be assessed using the following differential Equations (10) and (11):

$$\frac{dClim_i}{dt} = \frac{dClim_i}{dPM} \times \frac{dPM}{dt} + \frac{dClim_i}{dSO_2} \times \frac{dSO_2}{dt} + \frac{dClim_i}{dNO_2} \times \frac{dNO_2}{dt} + \frac{dClim_i}{dO_3} \times \frac{dO_3}{dt} \quad (10)$$

In the above Equation (10), $Clim_i$ means different climatic parameters such as precipitation, temperature maximum, and temperature minimum. This equation is based on the chain rule of calculus, which states that the derivative of a composite function (in this case, " $Clim_i$ " as a function of " PM , SO_2 , NO_2 , and O_3 " and " PM , SO_2 , NO_2 , and O_3 " as a function of time) is equal to the product of the derivatives of the individual functions. The equation suggests that the rate of change of a climate variable " $Clim_i$ " can be influenced by changes in an air pollutants " PM , SO_2 , NO_2 , and O_3 ". By understanding the relationship between these variables and their rates of change over time, we can gain insights into how

changes in one variable may influence the other. This equation is a simple representation of the complex interactions between the atmosphere, land, and oceans that determine the Earth's climate. It can be used to investigate the impacts of various human activities, such as emissions of air pollutants, on the climate system.

$$\Delta Clim_i = a \times \Delta PM + b \times \Delta SO_2 + c \times \Delta NO_2 + d \times \Delta O_3 \quad (11)$$

Equation (11) explains in general that ΔPM , ΔSO_2 , ΔNO_2 , and ΔO_3 are the inter-annual changes while a , b , c , and d mean coefficients.

3. Results

3.1. Trend Analysis of Air Pollution Variation under Pre- and Post-Scenarios

The current study presents the spatiotemporal characteristics of climatic variables and air pollutants from 2004 to 2021 using OMI, SEDAC, and ERA5 data. To analyze the spatial characteristics, we performed a trend analysis on the average annual concentrations of air pollutants from 2004 to 2021. We divided our study period into two scenarios based on APPCAP, namely pre- and post-scenarios, by accounting for the periods 2004–2013 and 2013–2021, respectively. We wanted to ensure the significance of the results of APPCAP in China. During the pre-scenario, it was observed that PM, SO_2 , and NO_2 showed heterogeneous trends, whereas the trend for O_3 was homogenous across the study area. Figure 4 shows the most prominent increasing trend for NO_2 , which was 1.21×10^{15} molecules/cm² per year. It is caused by anthropogenic emissions associated with economic growth, including traffic flow and urbanization [60].

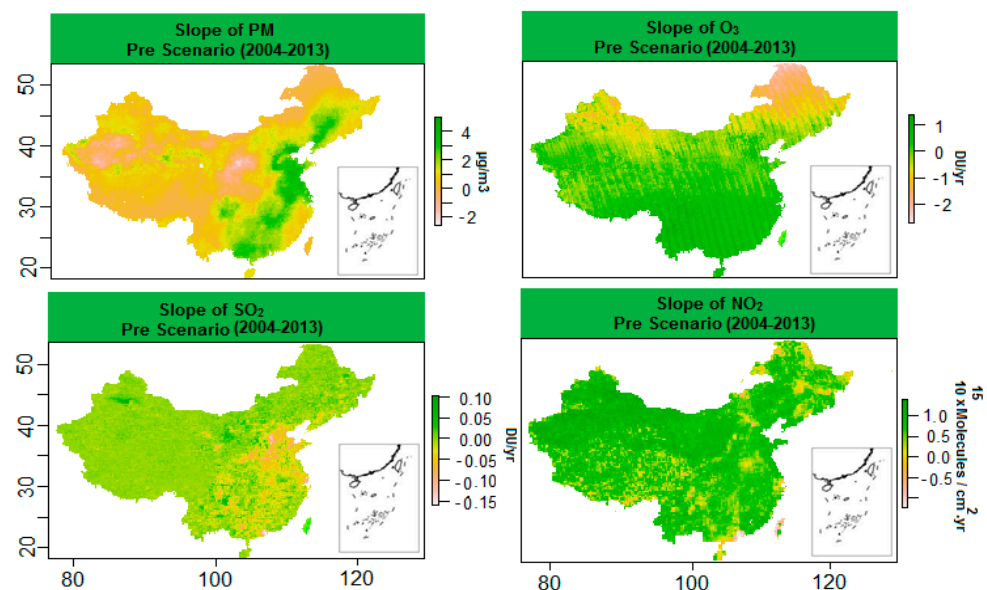


Figure 4. Slope of air pollutants for the pre-scenario (2004–2013).

In the case of PM and SO_2 , the increasing trend was 4 $\mu\text{gm}^{-3}/\text{year}$ and 0.1 DU/year, respectively, during 2004–2013. In the pre-scenario group, the highest increasing trend for PM was recorded in northeast, east, and southeast China. For O_3 , the trend over China was increasing, with the maximum value being 1 DU/year. On the other hand, the highest decreasing trend was recorded at 1.0×10^{15} molecules/cm² per year for NO_2 cross ponding to different hotspots in China.

The p values for PM and NO_2 were highly significant over most of the parts of the study region, as illustrated in Figure 5, whereas a mixed trend of p -value variation was observed for SO_2 and O_3 . After adopting the APPCAP (post-scenario), it was observed that PM and NO_2 showed a significantly decreasing trend in most of the part of China, whereas the trend for O_3 was still increasing in China.

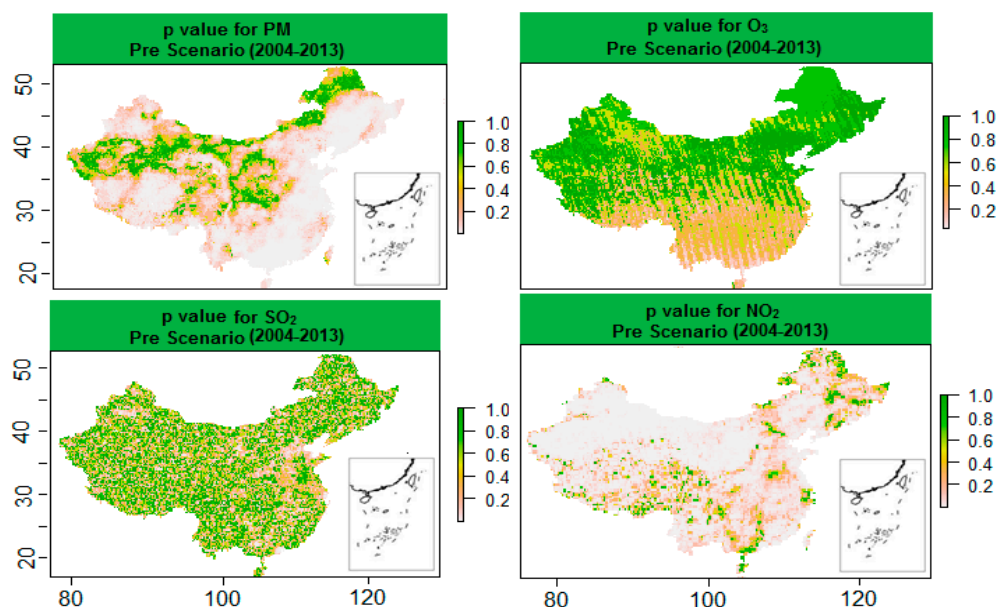


Figure 5. p Value of air pollutants for the pre-scenario period (2004–2013). Note: Mann Kendall p value at 95% confidence ($p < 0.05$).

Figure 6 shows the most prominent decreasing trend, as the trend for NO_2 was 1.21×10^{15} molecules/ cm^2 per year. In the northwest and north China, the trend was mixed for NO_2 , while the northeast China PM trend increased after adopting the APPCAP. In the case of O_3 , the trend decreased in the north part, while the rest of the area showed an increasing trend. The decreasing trend of O_3 was 2.0 DU/year during 2013–2021. In the post scenario, the trend for SO_2 was random, and a decreasing trend was found in central China, including the Shandong and Beijing areas. The highest decreasing trend for SO_2 was 0.10 DU/year, while the decreasing trend was recorded for PM in northeast, east, and southeast parts of China, with a peak value of $6 \mu\text{gm}^{-3}/\text{year}$. In contrast, O_3 showed an increasing trend with a maximum value of 1.2 DU/year. The highest increasing trends recorded were 0.05 DU/year and 1.21×10^{15} molecules/ cm^2 per year for SO_2 and NO_2 in China. From Figure 7, the p values showed that the decreasing trend for PM and NO_2 was highly significant in the study region, whereas the increment in O_3 pollution was highly significant during the post-scenario period.

3.2. Trend Analysis of Climatic Factors Variation under Pre and Post Scenarios

Figure 8 shows the spatial variation in trends for climatic parameters, including t_{max} , t_{min} , and precipitation. In general, all parameters showed an increasing trend across the study region. During the pre-scenario, t_{max} and t_{min} showed a prominent increasing trend, while precipitation showed a less significant increasing trend. t_{max} showed the maximum increasing trend of $0.30^\circ\text{C}/\text{year}$, while t_{min} represented $0.38^\circ\text{C}/\text{year}$. The precipitation trend also increased, but it was prominent in the north and southeast regions of China, where it increased by value 253 mm/year. However, a prominent decreasing trend was found along the Shandong region to the south part. The precipitation trend decreased by 72 mm/year. In the case of t_{max} , the trend did not significantly increase in the northern region, whereas t_{min} showed a decreasing trend in the same region of China. The maximum decreasing trend for t_{max} and t_{min} was $0.35^\circ\text{C}/\text{year}$ and $0.42^\circ\text{C}/\text{year}$, respectively. The trend variation in t_{max} , t_{min} , and precipitation was highly significant at $p < 0.05$ across the study area, as shown in Figure 9. After adopting the APPCAP, the trend variation was in contrast to the pre-scenario trend analysis results. Precipitation and t_{max} showed increasing trends with maximum trend values of 246 mm/year and $0.54^\circ\text{C}/\text{year}$, respectively. The t_{min} trend seemed to slightly increase by $0.61^\circ\text{C}/\text{year}$, especially in the north and southwest parts of China. In contrast, the precipitation trend decreased by 135 mm/year, particularly

in the southeast part of China. Furthermore, t_{\max} and t_{\min} showed a decreasing trend over 2013–2021 with a magnitude of $0.26\text{ }^{\circ}\text{C}/\text{year}$ and $0.37\text{ }^{\circ}\text{C}/\text{year}$, respectively.

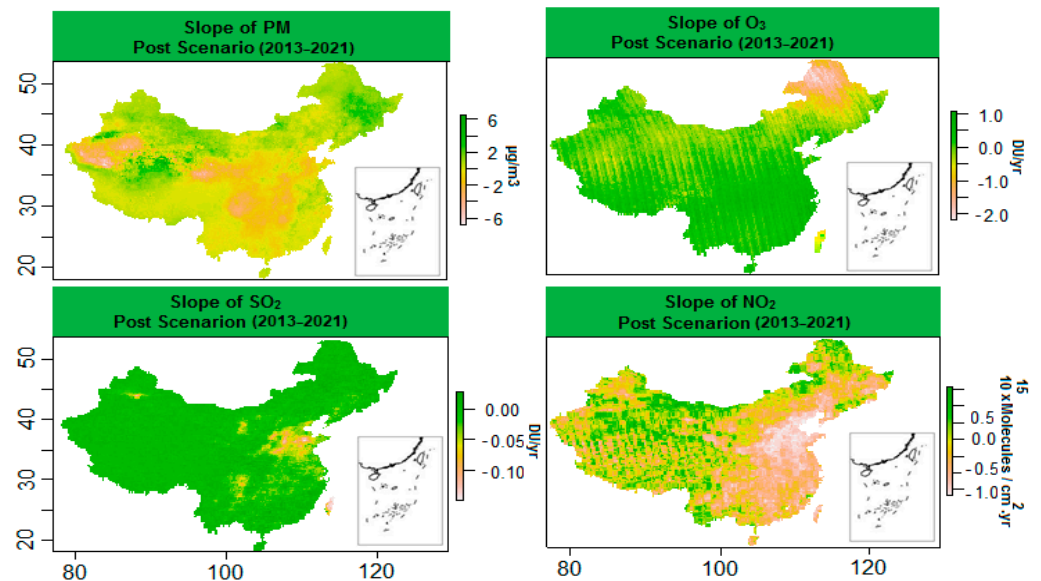


Figure 6. Slope of air pollutants for the post-scenario period (2013–2021).

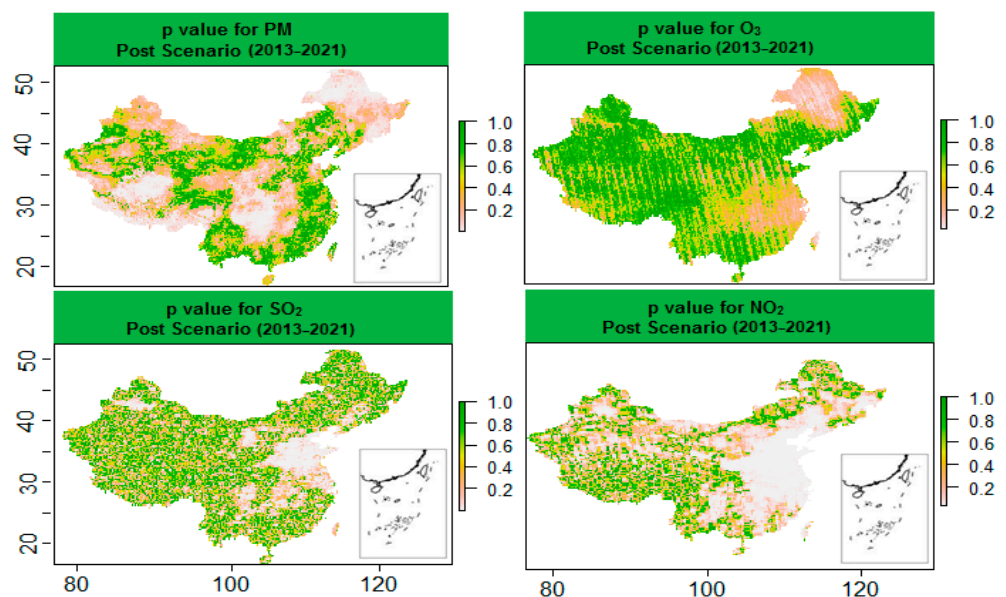


Figure 7. p value of air pollutants for the post-scenario period (2013–2021). Note: Mann Kendall p -value at 95% confidence ($p < 0.05$).

3.3. ITA Analysis for Air Pollution Variation under Pre and Post Scenarios

The annual variations in air pollutants were studied to analyze the impact of APPCAP on air pollution reduction. The ITA analysis showed an increasing or decreasing trend over two decades, during pre-scenario and post-scenario periods. A combination of increasing and decreasing trends for data points above the 5% range from the 1:1 line exhibited a significant trend. The results showed that, overall, NO_2 , PM, and SO_2 decreased after adopting APPCAP across China. Figure 10 suggests that air pollutants (NO_2 , PM, SO_2 , and O_3) significantly decreased. The results also showed that NO_2 data points fell within the -5% range, showing a decreasing trend during 2004 and 2021. The statistics for NO_2 exhibited significant negative values of ITA D. The O_3 data points were mostly on the diagonal line, indicating no trend/zero trends. The SO_2 data points fell above -5% ,

indicating that it decreased after adopting APPCAP. However, it was concluded that the decreasing trend of SO_2 was not significant over the period.

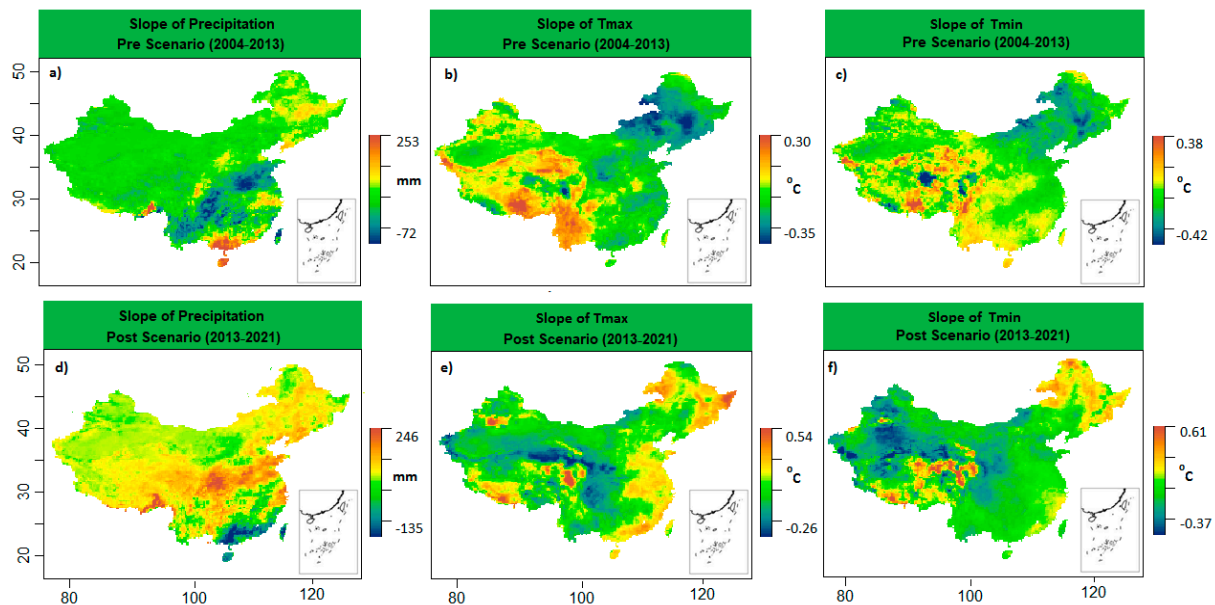


Figure 8. Slope of climatic variables for the pre- (a–c) and post- (d–f) scenarios over China.

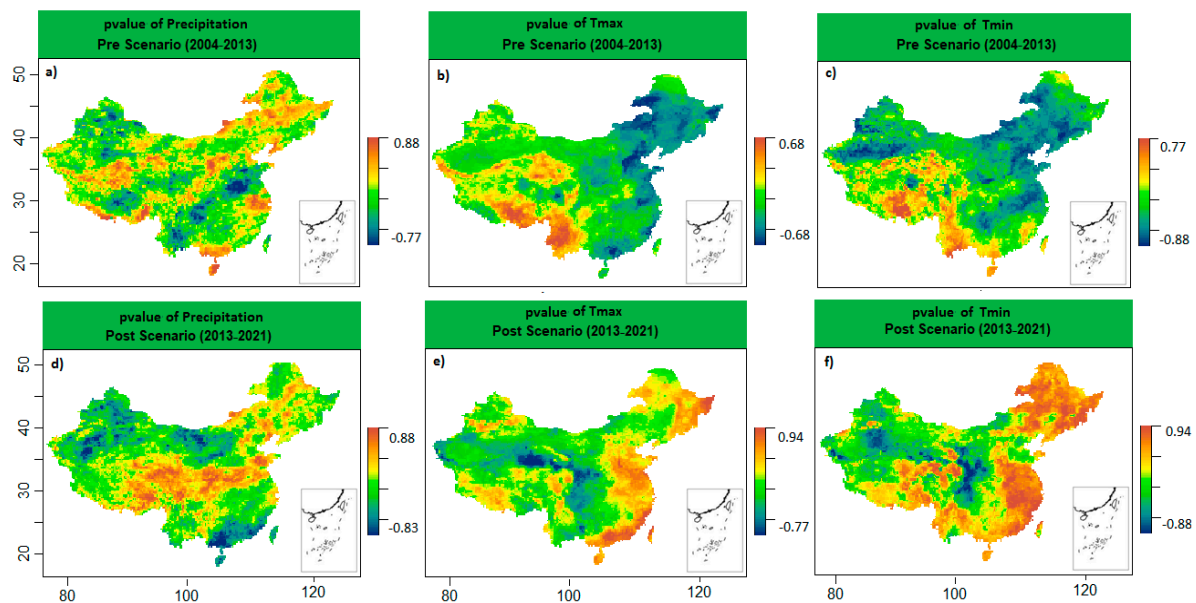


Figure 9. p value of climatic variables for pre- (a–c) and post- (d–f) scenarios over China. Note: Mann Kendall p value at 95% confidence ($p < 0.05$).

3.4. Impact Analysis of Air Pollutants on Climatic Factors before and after APPCAP

The impact analysis of air pollutants was investigated using the GWR model and differential Equations (8)–(11). We performed a spatial distribution analysis on the outputs from the differential equations to investigate the climatic impact of air pollution over two scenarios based on APPCAP in China.

3.4.1. Air Pollutant's Contribution to Temperature Maximum Patterns

The spatial characteristics of the contribution of air pollutants to t_{\max} patterns for the pre-scenario and post-scenario periods are represented in Figure 11. Higher positive values

show a greater influence on increasing t_{\max} over the study period. For the pre-scenario period, NO_2 had a higher value and increased t_{\max} by 2.42°C , while O_3 had a lower positive value of 1.10°C over a decade. In the case of SO_2 , the contribution pattern was random. In contrast, SO_2 had higher negative values and decreased t_{\max} by 2.07°C , while PM showed the lowest negative contribution with 0.55°C over China. PM caused an increase in t_{\max} in central east and southeast parts of China, as shown in Figure 11a. After adopting the APPCAP (post-scenario), PM showed the highest positive contribution to increasing t_{\max} by 1.80°C , while O_3 contributed the lowest positive value of 0.60°C . SO_2 showed random spatial patterns of increasing or decreasing t_{\max} over the whole study area. NO_2 contributed more to decreasing t_{\max} by 2.27°C , and spatial patterns showed that central east China was reducing t_{\max} , as shown in Figure 11h.

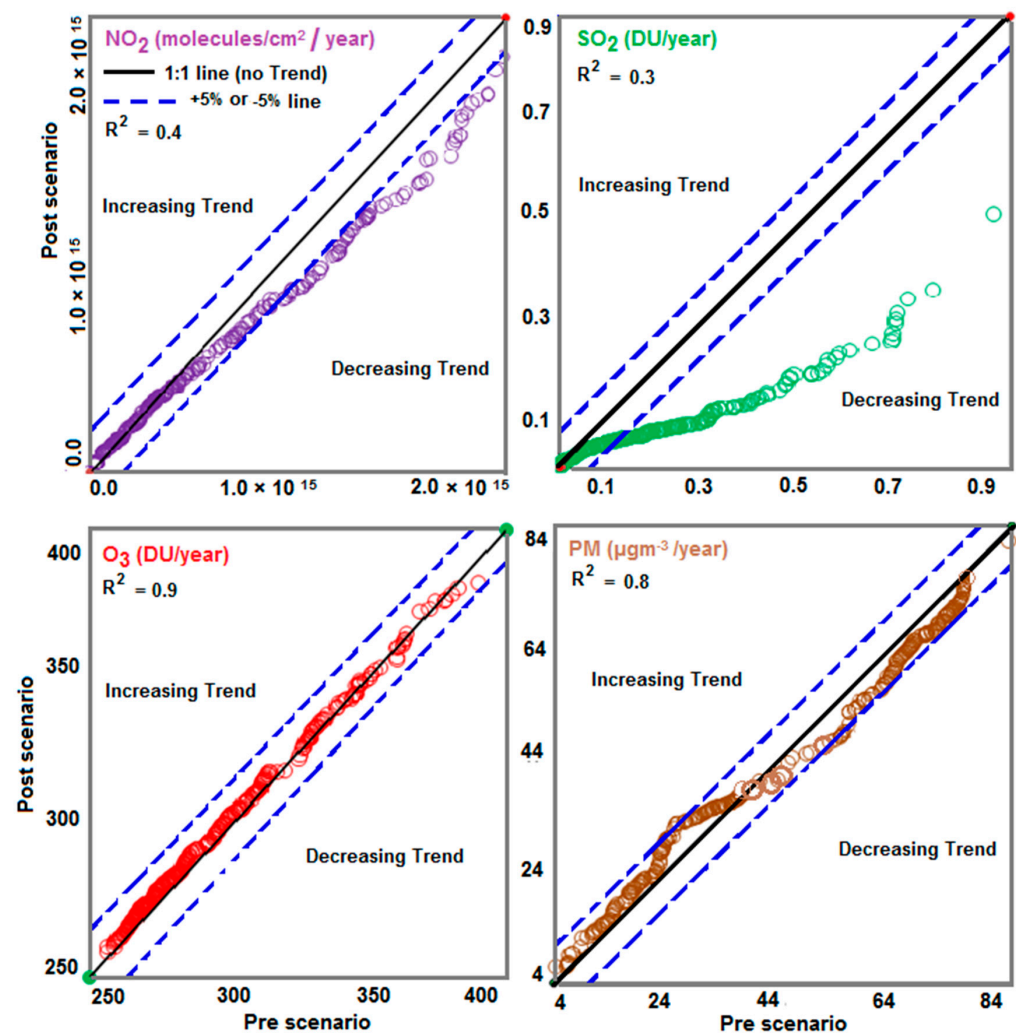


Figure 10. ITA trend of the pollutants (NO_2 , PM, SO_2 , and O_3). Note: Blue dotted line shows significance at ($p < 0.05$).

O_3 reduced t_{\max} in the southern part of China. The contribution pattern of O_3 indicated the lowest negative contribution to decreasing t_{\max} by 0.47°C . In general, a comparison of all air pollutant's contributions indicated that, during the pre-scenario period, t_{\max} positively changed by 2.42°C , followed by NO_2 , while in the post-scenario period, t_{\max} positively changed by 1.80°C , followed by PM. In contrast, the highest negative t_{\max} change was by 2.07°C , followed by SO_2 , and 2.27°C followed by NO_2 , respectively. NO_2 and PM particles can contribute to global warming by trapping the heat in the atmosphere. They cause the warming effect on the atmosphere by absorbing the sunlight and re-emitting it as heat, leading to a rise in the temperature. The current effect is more in urbanized areas,

where there are high traffic and industrial emissions. Further, NO_2 may also react with chemicals in the atmosphere to form secondary pollutants such as O_3 , which can increase warming. Moreover, O_3 leads to an increase in temperature. SO_2 is primarily released from the burning process and volcanic eruption. It has harmful effects on human health as well as the environment. However, SO_2 emissions contribute to warming the atmosphere because it can react with other chemicals in the atmosphere to form sulfate aerosols and lead to an increase in temperature. This effect is more prominent in areas with high concentrations of SO_2 , such as power and industrial plants. Overall, the pollutants significantly impact the temperature maximum, particularly in areas with high concentrations. The effect of the air pollutants on t_{\max} depends on the concentration level, size of the particles, as well as other factors such as location and weather conditions.

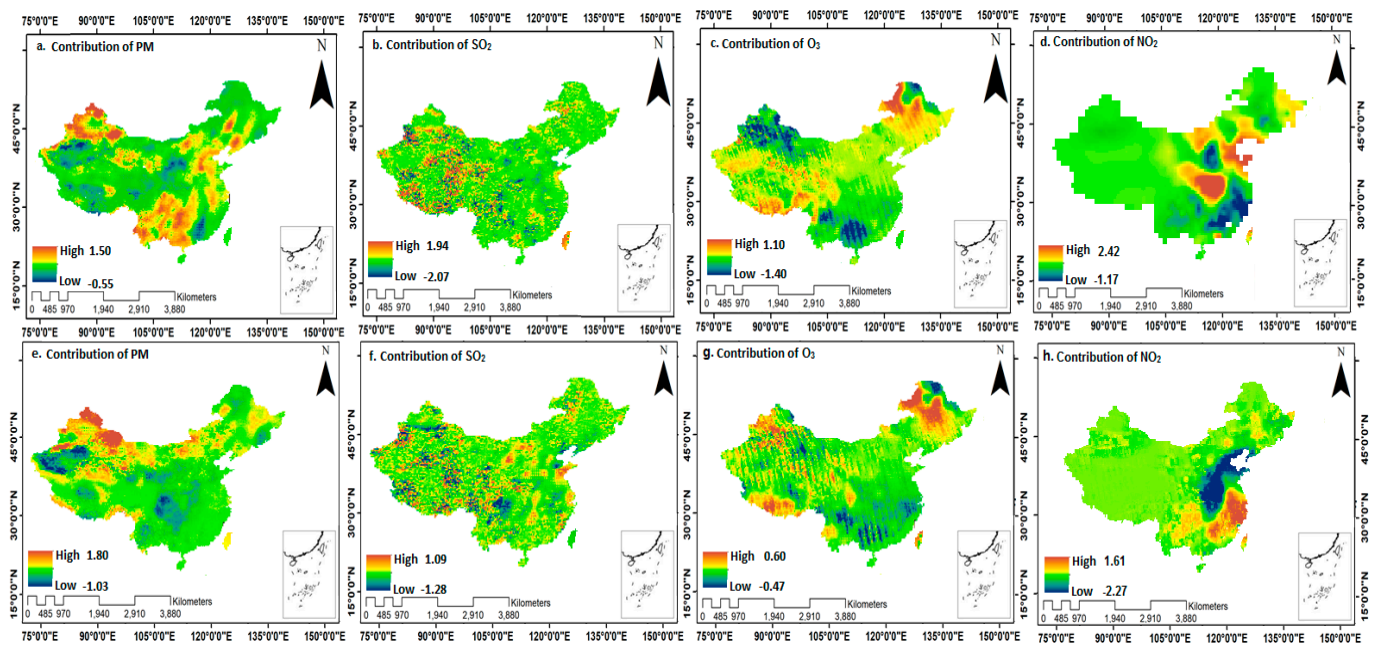


Figure 11. Contribution of air pollutants to temperature maximum ($^{\circ}\text{C}$) pattern changes. Note: Pre-scenario (a–d) and Post-scenario (e–h).

3.4.2. Air Pollutant Contribution to Temperature Minimum Patterns

In this section, the spatial characteristics of the contribution to t_{\min} changes for the pre-scenario and post-scenario periods are represented in Figure 12, which shows the spatially interpolated geographical air pollution contribution to climatic factors (t_{\min}). The northern, western, and southeastern parts of China indicated a position association with air pollutants during the pre-scenario period (2004–2013). Figure 12a,d shows the higher positive influence on increasing t_{\min} by 2.19°C , followed by SO_2 , while NO_2 had the second highest contribution to change in t_{\min} by 1.96°C during the pre-scenario period. The northeastern and southern parts indicated the rise in t_{\min} due to the variation in PM. NO_2 caused higher t_{\min} changes over the north, central, and southeast parts of China. In contrast, NO_2 contributed to a higher negative contribution to decrease t_{\min} by 2.24°C , while PM had a lower negative contribution with a value of 0.43°C over a decade. Figure 12d indicates that NO_2 was mainly responsible for decreasing t_{\min} mainly in the central part of China. O_3 and SO_2 had mixed patterns for changing t_{\min} (Figure 12b,c).

In the post-scenario period, the west, north, and central parts of China showed an increasing contribution to t_{\min} changes. NO_2 showed the highest positive contribution to increasing t_{\min} by 2.24°C , while O_3 had the lowest positive contribution with 0.60°C . The second highest positive contribution to increasing t_{\min} was with PM (1.69°C). SO_2 and O_3 showed random spatial patterns to increase or decrease t_{\min} over the whole study area. NO_2 had a positive contribution in central east China, as shown in Figure 12h. In contrast,

NO₂ had the highest negative contribution for reducing t_{\min} by 1.53 °C in the northeast and southeast parts of China.

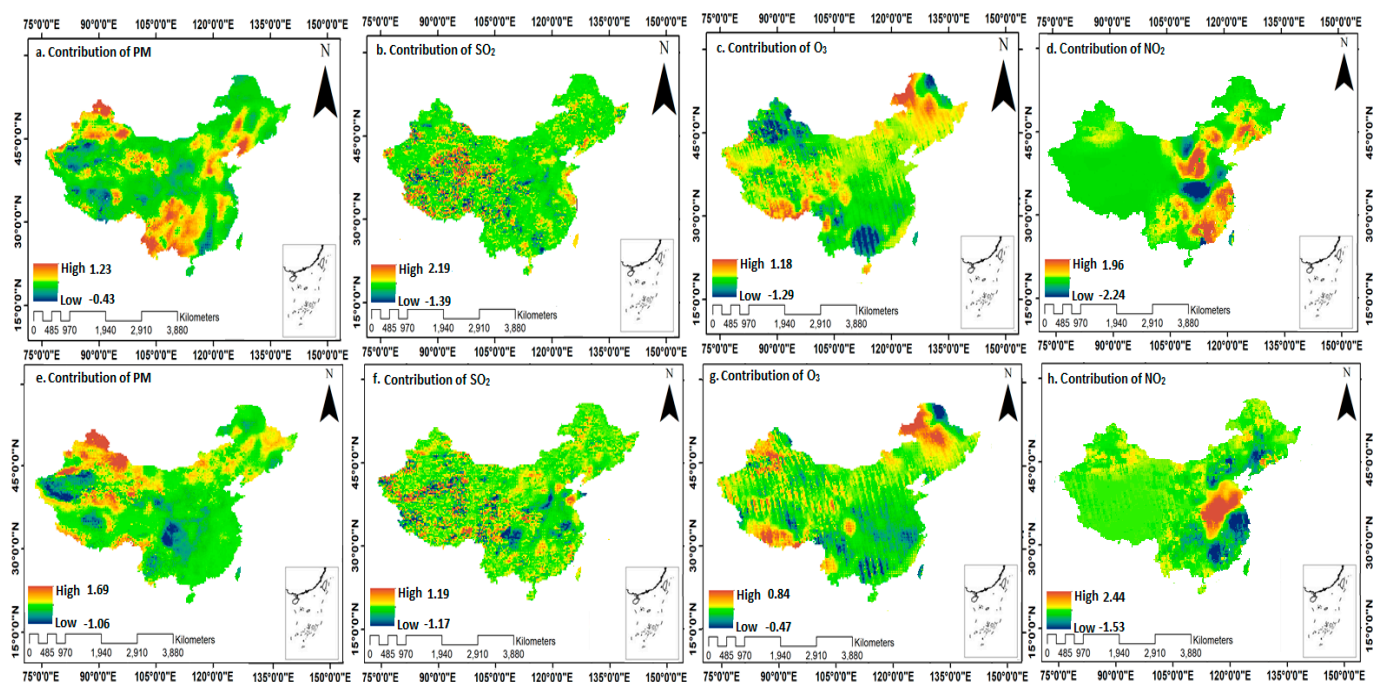


Figure 12. Contribution of air pollutants to temperature minimum (°C) pattern changes. Note: Pre-scenario (a–d) and Post-scenario (e–h).

Moreover, O₃ contribution patterns indicated the lowest negative contribution to decreasing the t_{\min} by 0.47 °C. O₃ reduced t_{\min} in the east-southeast part of China during the post-scenario period. Overall, a comparison of all air pollutants contributions indicated that, during the pre-scenario and post-scenario periods, the t_{\min} changed the highest positively by 2.19 °C followed by the SO₂, while it was 2.44 °C followed by NO₂ during the pre-scenario period. In contrast, t_{\min} has the highest negative change by 2.24 °C, while it was 1.53 °C followed by NO₂ in the case of the pre- and post-scenario periods, respectively. NO₂ has direct and indirect impacts on temperature minimum. It can have a warming effect. NO₂ absorbs sunlight and heat in the atmosphere that can lead to an increase in temperature, especially at night. It is important to note that impacts of SO₂ on t_{\min} depend on the different factors such as season and altitude. The sulfate aerosols reflect solar radiation and reduce the energy on the Earth's surface. This phenomena causes a cooling effect on temperature, including t_{\min} . Moreover, NO₂ causes the urban heat island effect, where cities experience higher temperatures than surrounding rural areas due to human activity and the built environment. This effect can further increase the minimum temperature in urban areas, leading to a range of health and environment impacts.

This warming effect can have several consequences, including the melting of snow and ice, changes in precipitation patterns, and alternations in plant growth and ecosystem functioning.

3.4.3. Air Pollutant Contribution to Precipitation Patterns

Figure 13 shows spatial maps of the contribution of air pollutants in changing precipitation patterns over China in the pre- and post-scenario periods. Figure 13b,c shows the highest positive influence on precipitation, with an increase of 40 mm, followed by SO₂, while O₃ had the second highest contribution to changes in precipitation, with an increase of 39 mm during the pre-scenario period. The central-eastern part indicates the rise in precipitation due to variations in SO₂, while O₃ caused higher precipitation changes over the Southern part of China. In contrast, SO₂ had a negative contribution to decreasing

precipitation by 22 mm, while NO_2 had lowest negative contribution, with a value of 0.01 mm over a decade. Figure 13b,d indicates the lower precipitation hotspots in the south of China caused by SO_2 , while NO_2 showed hotspots in the east of China, respectively.

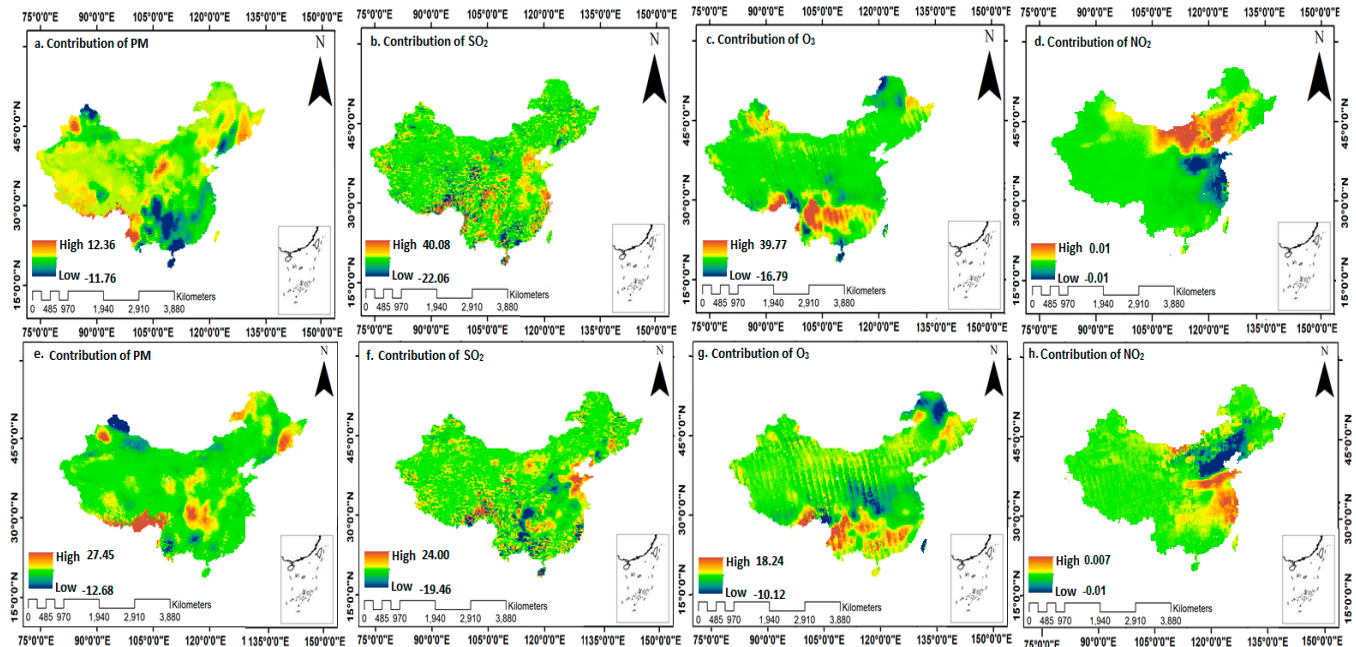


Figure 13. The contribution of air pollutants to precipitation (mm) pattern changes. Note: Pre-scenario (a–d) and Post-scenario (e–h).

In the post-scenario period, the south, east, and central parts of China showed increasing contributions to precipitation alteration. PM made the highest positive contribution to increasing the precipitation by 27 mm, while NO_2 had the lowest positive contribution, with 0.007 mm. The second-highest positive contribution to raising precipitation was with SO_2 (24 mm). The PM contribution was positive in the central part of China, as shown in Figure 13e. In contrast, SO_2 had the highest negative contribution to reducing the precipitation magnitude by 19 mm in the central east (Shandong) part of China. Moreover, NO_2 contribution patterns indicated the lowest negative contribution to reducing precipitation by 0.01 mm. NO_2 reduced the precipitation in the north part of China during the post-scenario (2013–2021). Overall, a comparison of all air pollutant contributions indicated that during the pre-scenario period, the highest positive precipitation change was by 40 mm followed by SO_2 , while it was 27 mm followed by PM in the case of the post-scenario period. In contrast, the highest negative precipitation change was by 22 mm, while it was 19 mm followed by SO_2 during the pre- and post-scenario periods, respectively. SO_2 and PM had significant impacts on the precipitation pattern and environment. SO_2 reacts with other chemicals to produce sulfate aerosols that may affect precipitation in different ways. SO_2 affects the precipitation pattern by altering the formation of clouds. Sulfate aerosols act as cloud condensation nuclei, which are important for the formation of clouds. PM particles promote the formation of clouds and change their properties through cloud condensation nuclei. However, these particles may affect the properties of clouds, including droplet size, their reflectivity, and the amount of precipitation they produce. As a result, the timing of precipitation as well as the pattern is affected. Additionally, SO_2 may impact precipitation patterns through its interactions with other atmospheric chemicals.

As an example, SO_2 reacts with nitrogen oxides to create fine PM particles that significantly affect precipitation patterns, in particular, the areas with high concentrations of both SO_2 and NO_x . PM emissions from urban and industrial areas can lead to forming urban heat islands, which alter local wind patterns and precipitation by changing the moisture content and temperature of the air.

4. Discussion

The State Council issued an action plan, APPCAP, to combat air pollution in 2013, which became the most ambitious policy to control air pollution concentrations [30,72]. APPCAP aimed to improve the following aspects: (1) control air pollution, (2) control pollution substances, (3) diversify air pollution control strategies, and (4) optimize pollution management mode [71,96,97]. The current study divided the entire study period into two separate scenarios to better comprehend the promising efforts of China: the pre-scenario (before APPCAP) and post-scenario (after APPCAP) periods. The APPCAP is a significant development in China's efforts to curb air pollution, and motivates researchers to assess the implications of air pollution's management at the national level. MK trend analysis was performed before and after APPCAP implementation on mean annual data. ITA is an intuitive method used to identify trends in different time series subcategories and can be applied irrespective of distribution assumptions [85–87], while the MK test assumes that time series have no sequence correlation and are least-based and all data are significant [88]. During the pre-scenario period, trend analysis results on PM, SO₂, and NO₂ showed heterogeneous trends, whereas the trend for O₃ was homogenous. The most prominent increase in NO₂ concentration was 1.21×10^{15} molecules/cm² per year [64,98,99]. In the case of PM and SO₂, the increasing trend was 4 µgm⁻³/year and 0.1 DU/year [88]. Northeastern, eastern, and southeastern China showed the highest increasing trend for PM in the pre-scenario period. For O₃, the trend increased across the region with a maximum value of 1 DU/year in the pre-scenario period.

In light of stringent clean air pollution actions, including APPCAP, adopted in China since 2013 (post-scenario), data analysis showed that PM and NO₂ had significantly decreasing trends in most of China, while the trend for O₃ did not reduce considerably and is still escalating [100,101]. In the post-scenario period, Beijing, Shandong, and other areas of central China showed a random and declining tendency for SO₂ [102], with the greatest rate of decline for SO₂ being 0.10 DU/year.

The spatial variation of the trend for the climatic parameters, including t_{\max} , t_{\min} , and precipitation, increased across the study region. During the pre-scenario period, t_{\max} showed a decreasing mean annual trend of 0.025 °C/year, and t_{\min} represented 0.02 °C/year, respectively, while precipitation had an increasing mean annual trend by a value of 90 mm/year. After adopting the APPCAP, trend variation was in contrast to the pre-scenario period for temperature trend analysis results. During the post scenario period, precipitation, t_{\max} , and t_{\min} showed increasing mean annual trends by 55 mm/year, 0.14 °C/year, and 0.12 °C/year, respectively, and were highly significant at ($p < 0.05$). Overall, t_{\max} and t_{\min} increased while the precipitation reduced.

A comparison of the effects of air pollution on climate between the pre- and post-scenario periods was analyzed for a two-decade period using ITA to determine whether there was an increasing or decreasing trend. The results showed that, when China adopted the APPCAP, overall concentrations of NO₂, SO₂, and PM declined. Figure 10 indicates that the levels of airborne pollutants (NO₂, SO₂, and PM) dramatically decreased. NO₂ data values above the −5% range showed a declining trend between 2013 and 2021, and NO₂ statistics exhibited significant negative values for ITA. However, despite the massive reduction in NO_x emissions from power plants, vehicle emissions continued to increase. Both on- and off-road vehicles significantly contribute to air pollution, and multiple studies have revealed a strong correlation between rising vehicle traffic and air pollution in Chinese megacities [103–106]. Since the 1990s, the central government has implemented integrated emission control policies to reduce vehicle emissions, including emission standards for new vehicles, emission controls for existing vehicles, modifications in fuel quality, the promotion of advanced vehicles, sustainable transportation, and traffic management programs [107].

O₃ data points mostly fall on the (1:1) line, indicating no trend/zero trends. According to Liu [108], the sources of the ozone and its variation in concentrations in China, substantial declines in PM, and SO₂ emissions lead to a rise in urban O₃ due to the dynamic interaction between aerosols, radiation, and chemical reactions. O₃ concentrations also increase in the

southwest due to climatic factors [109]. Additionally, several studies found that reducing the concentration of NO_x increases the amount of O₃. During the COVID-19 lockdown, the transportation sector shutdown resulted in a reduction in NO_x, which decreased the neutralization of NO into O₃, which raised the concentration of O₃ [110,111].

The SO₂ data points were above −5%, indicating that it started to decline after the APPCAP was implemented. Additionally, it was determined that the decreasing tendency of SO₂ over the period was significant and it was in line with findings of [97]. China's environmental regulations resulted in significant reductions in SO₂ emissions, but overall, coal consumption has continued to rise. Since 1996, reducing SO₂ emissions from major industries, including coal-fired thermal power and iron/steel plants, has been top priority. The installation and strict management of online monitoring equipment in the main industries have become mandatory, and different policies and programs have been implemented during previous Five-Year Plans [107,112].

Our study has certain limitations. We examined the long-term changes in air pollutants and climatic factors, as well as their association based on different statistical models. The APPCAP adaptation resulted in an increase in t_{\min} and precipitation. The rise in t_{\min} may result in local warming in China for the most part, which requires more efforts to combat climatic change. To this end, there is a need to focus on the mechanisms underlying these regional climate changes, based on seasonal variation. The climatic effect of air pollution along seasonal variation remains unexplored, and coupling regional climate models to analyze the radiative effects of China's emission reductions.

Climatic Impact of Air Pollutants for Pre and Post Scenarios

The current study describes the climatic changes due to variations in air pollutants in response to the adoption of the APPCAP. In the pre-scenario period, most of the air pollutants showed positive contributions to changing the climate. For example, O₃ played a role in reducing t_{\max} (t_{\min}) with a value of 0.15 °C (0.05 °C) and increasing precipitation with a value of 11mm, as shown in Table 2. PM showed a positive relationship with all climatic parameters with values of 0.47 °C (t_{\max}), 0.41 °C (t_{\min}), and 0.31 mm (precipitation). The analysis showed that NO₂ had positive and negative relationships with t_{\max} (precipitation) 0.62 °C (0.1mm) and t_{\min} (0.14 °C), respectively. SO₂ showed an increasing contribution with t_{\min} (precipitation) 0.41 °C (9mm), while decreasing with t_{\max} (0.06 °C).

Table 2. An average value of climatic variation in response to air pollutant changes during (pre- and post-) scenarios in the study area.

APPCAP	Parameter	T_{\max} °C	T_{\min} °C	Precp mm
Pre-Scenario	NO ₂	0.62	−0.14	0.0
	PM	0.47	0.41	0.31
	SO ₂	−0.06	0.41	9
	O ₃	−0.15	−0.05	11
Post-Scenario	NO ₂	−0.33	0.45	0.001
	PM	0.38	0.31	7.38
	SO ₂	−0.09	0.02	2.27
	O ₃	0.06	0.18	4.06

During 2013–2021 (post scenario), most of the air pollutants (PM, SO₂) showed positive contributions to alter the climatic pattern including t_{\max} , t_{\min} , and precipitation. The analysis showed that PM had a positive relationship with t_{\max} (t_{\min}) 0.38 °C (0.31 °C), and precipitation (7.38 mm). NO₂ showed an increasing contribution with t_{\min} (precipitation) 0.35 °C (0.001 mm), while decreasing with t_{\max} (0.33 °C). Moreover, SO₂ indicated an increasing contribution to t_{\min} (precipitation) 0.02 °C (2.2 mm), while decreasing with t_{\max} (0.09 °C).

5. Conclusions

In summary, when China adopted the APPCAP, NO₂, SO₂, and PM concentrations declined dramatically. According to ITA, NO₂ data values above the −5% range showed significant declining trend between 2013 and 2021. Although O₃ concentrations have gradually increased, the air quality in most cities has immensely improved as a result of the stringent control measures by the State Council. The O₃ data points are mostly on the (1:1) line, which means that there is no trend/zero trends. The decreasing tendency of SO₂ over the period is not significant. Despite the tremendous progress made in reducing air pollution, PM and O₃ concentrations continue to be considerably above WHO guidelines. More efforts are required to focus on the research and development of new methods to address these ongoing challenges in air pollution emissions. The MK test investigated that all pollutants showed an increasing trend for pre-APPCAP, while showing a decreasing trend, except for O₃, during the post-APPCAP period. For climatic factors, the MK test showed an increasing trend of precipitation and t_{\min} for the post-APPCAP period.

We used GWR and differential equation models to identify the climatic impact of air pollution before and after the implementation of APPCAP in 2013 to combat air pollution. Two scenarios based on APPCAP were made to account for the air pollution variation in China during 2004–2021. The contributions of the most influential air pollutants were calculated using the GWR and differential equation models. In the pre-scenario period, NO₂ contributed to increasing the mean maximum air temperature (t_{\max}) by 0.62 °C, PM contributed to raising t_{\min} by 0.41 °C, while O₃ reduced t_{\max} (t_{\min}) by 0.15 °C (0.05 °C). PM increased t_{\max} and precipitation with magnitudes of 0.38 °C and 7.38mm, respectively, while NO₂ contributed to increasing t_{\min} by 0.35 °C during the post-scenario period. In particular, the post-scenario period led to increases in t_{\min} and precipitation across the country. The current study findings explain the significance of APPCAP and its role in changing the regional climate of China. Policymakers must implement measures to reduce emissions and maintain the climate warming level across the region. In the future, China needs to introduce more renewable energy to dominate the coal energy system, which may help with national and international climate mitigation measures.

Author Contributions: Conceptualization, B.C. and A.D.; methodology, A.D.; software, A.D.; validation, A.D.; formal analysis, A.D.; investigation, A.D.; resources, B.C.; data curation, A.D., M.H., M.A., A.A., Z.U.-H., M.G., M.S., J.F., H.Z. and B.S.; writing—original draft preparation, A.D.; writing—review and editing, A.D. and B.C.; visualization, A.D.; supervision, B.C.; project administration, B.C.; funding acquisition, B.C. All authors have read and agreed to the published version of the manuscript.

Funding: This research was funded by National Key R&D Program of China (2018YFA0606001) and National Natural Science Foundation of China (41771114).

Data Availability Statement: No new data were created.

Acknowledgments: The first author wants to thank <https://giovanni.gsfc.nasa.gov/> (accessed on 20 February 2023), <https://sedac.ciesin.columbia.edu> (accessed on 20 February 2023), Fifth generation (ERA5) <https://www.ecmwf.int/en> (accessed on 20 February 2023), and <http://www.aqistudy.cn/> (accessed on 20 February 2023) for providing the open access data and the Ministry of Ecology and Environment, China, for data (<http://www.aqistudy.cn/> (accessed on 20 February 2023)) available from 2013.

Conflicts of Interest: The authors declare no conflict of interest.

References

1. Tang, K.H.D. Climate change in Malaysia: Trends, contributors, impacts, mitigation and adaptations. *Sci. Total Environ.* **2019**, *650*, 1858–1871. [CrossRef] [PubMed]
2. Destek, M.A.; Sarkodie, S.A. Investigation of environmental Kuznets curve for ecological footprint: The role of energy and financial development. *Sci. Total Environ.* **2019**, *650*, 2483–2489. [CrossRef] [PubMed]
3. Ira, S. Modeling of Land Surface Temperature (LST) and Normalized Difference Vegetation Index (NDVI) in Nepal: 2000–2015. Ph.D. Thesis, Prince of Songkla University, Pattani Campus, Thailand, 2018.

4. Harold, J.; Lorenzoni, I.; Shipley, T.F.; Coventry, K.R. Communication of IPCC visuals: IPCC authors' views and assessments of visual complexity. *Clim. Chang.* **2020**, *158*, 255–270. [\[CrossRef\]](#)
5. Liu, Y.; Shao, T.; Hua, S.; Zhu, Q.; Luo, R. Association of anthropogenic aerosols with subtropical drought in East Asia. *Int. J. Climatol.* **2020**, *40*, 3500–3513. [\[CrossRef\]](#)
6. Yang, Y.; Ren, L.; Wu, M.; Wang, H.; Song, F.; Leung, L.R.; Hao, X.; Li, J.; Chen, L.; Li, H. Abrupt emissions reductions during COVID-19 contributed to record summer rainfall in China. *Nat. Commun.* **2022**, *13*, 959. [\[CrossRef\]](#)
7. Liu, Z.; Zhan, W.; Bechtel, B.; Voogt, J.; Lai, J.; Chakraborty, T.; Wang, Z.-H.; Li, M.; Huang, F.; Lee, X. Surface warming in global cities is substantially more rapid than in rural background areas. *Commun. Earth Environ.* **2022**, *3*, 219. [\[CrossRef\]](#)
8. Xiao, B.; Bowker, M.A. Moss-biocrusts strongly decrease soil surface albedo, altering land-surface energy balance in a dryland ecosystem. *Sci. Total Environ.* **2020**, *741*, 140425. [\[CrossRef\]](#)
9. Letcher, T.M. Why do we have global warming? In *Managing Global Warming*; Elsevier: Amsterdam, The Netherlands, 2019; pp. 3–15.
10. Raimi, M.O.; Vivien, O.T.; Oluwatoyin, O.A. Creating the healthiest nation: Climate change and environmental health impacts in Nigeria: A narrative review. *Sch. Sustain. Environ.* **2021**, *6*. [\[CrossRef\]](#)
11. Wang, Z.; Zhang, M.; Wang, L.; Qin, W.; Ma, Y.; Gong, W.; Yu, L. Investigating the all-sky surface solar radiation and its influencing factors in the Yangtze River Basin in recent four decades. *Atmos. Environ.* **2021**, *244*, 117888. [\[CrossRef\]](#)
12. Lean, J.; Rind, D. Climate forcing by changing solar radiation. *J. Clim.* **1998**, *11*, 3069–3094. [\[CrossRef\]](#)
13. Seppälä, A.; Matthes, K.; Randall, C.E.; Mironova, I.A. What is the solar influence on climate? Overview of activities during CAWSES-II. *Prog. Earth Planet. Sci.* **2014**, *1*, 24. [\[CrossRef\]](#)
14. Heaviside, C.; Witham, C.; Vardoulakis, S. Potential health impacts from sulphur dioxide and sulphate exposure in the UK resulting from an Icelandic effusive volcanic eruption. *Sci. Total Environ.* **2021**, *774*, 145549. [\[CrossRef\]](#) [\[PubMed\]](#)
15. Babu, S.R.; Liou, Y.-A. Day-to-day variability of upper troposphere and lower stratosphere temperature in response to Taal volcanic eruption inferred from COSMIC-2 RO measurements. *J. Volcanol. Geotherm. Res.* **2022**, *421*, 107445. [\[CrossRef\]](#)
16. Yang, J.; Wang, Y.; Xiu, C.; Xiao, X.; Xia, J.; Jin, C. Optimizing local climate zones to mitigate urban heat island effect in human settlements. *J. Clean. Prod.* **2020**, *275*, 123767. [\[CrossRef\]](#)
17. Li, X.; Stringer, L.C.; Chapman, S.; Dallimer, M. How urbanisation alters the intensity of the urban heat island in a tropical African city. *PLoS ONE* **2021**, *16*, e0254371. [\[CrossRef\]](#)
18. Silva, J.S.; da Silva, R.M.; Santos, C.A.G. Spatiotemporal impact of land use/land cover changes on urban heat islands: A case study of Paço do Lumiar, Brazil. *Build. Environ.* **2018**, *136*, 279–292. [\[CrossRef\]](#)
19. Dilawar, A.; Chen, B.; Trisurat, Y.; Tuankruea, V.; Arshad, A.; Hussain, Y.; Measho, S.; Guo, L.; Kayiranga, A.; Zhang, H. Spatiotemporal shifts in thermal climate in responses to urban cover changes: A-case analysis of major cities in Punjab, Pakistan. *Geomat. Nat. Hazards Risk* **2021**, *12*, 763–793. [\[CrossRef\]](#)
20. Wright, L.P.; Zhang, L.; Cheng, I.; Aherne, J.; Wentworth, G.R. Impacts and effects indicators of atmospheric deposition of major pollutants to various ecosystems—A review. *Aerosol Air Qual. Res.* **2018**, *18*, 1953–1992. [\[CrossRef\]](#)
21. Saud, B.; Paudel, G. The threat of ambient air pollution in Kathmandu, Nepal. *J. Environ. Public Health* **2018**, *2018*, 1504591. [\[CrossRef\]](#)
22. Wang, J.; Liu, X.; Li, Y.; Powell, T.; Wang, X.; Wang, G.; Zhang, P. Microplastics as contaminants in the soil environment: A mini-review. *Sci. Total Environ.* **2019**, *691*, 848–857. [\[CrossRef\]](#)
23. Kumari, P.; Toshniwal, D. Impact of lockdown on air quality over major cities across the globe during COVID-19 pandemic. *Urban Clim.* **2020**, *34*, 100719. [\[CrossRef\]](#) [\[PubMed\]](#)
24. Donzelli, G.; Cioni, L.; Cancellieri, M.; Llopis Morales, A.; Morales Suárez-Varela, M.M. The effect of the Covid-19 lockdown on air quality in three Italian medium-sized cities. *Atmosphere* **2020**, *11*, 1118. [\[CrossRef\]](#)
25. Agarwal, N.; Meena, C.S.; Raj, B.P.; Saini, L.; Kumar, A.; Gopalakrishnan, N.; Kumar, A.; Balam, N.B.; Alam, T.; Kapoor, N.R. Indoor air quality improvement in COVID-19 pandemic. *Sustain. Cities Soc.* **2021**, *70*, 102942. [\[CrossRef\]](#) [\[PubMed\]](#)
26. Glencross, D.A.; Ho, T.-R.; Camina, N.; Hawrylowicz, C.M.; Pfeffer, P.E. Air pollution and its effects on the immune system. *Free Radic. Biol. Med.* **2020**, *151*, 56–68. [\[CrossRef\]](#) [\[PubMed\]](#)
27. Domingo, J.L.; Marquès, M.; Rovira, J. Influence of airborne transmission of SARS-CoV-2 on COVID-19 pandemic. A review. *Environ. Res.* **2020**, *188*, 109861. [\[CrossRef\]](#) [\[PubMed\]](#)
28. Dong, W.; Liu, S.; Chu, M.; Zhao, B.; Yang, D.; Chen, C.; Miller, M.R.; Loh, M.; Xu, J.; Chi, R. Different cardiorespiratory effects of indoor air pollution intervention with ionization air purifier: Findings from a randomized, double-blind crossover study among school children in Beijing. *Environ. Pollut.* **2019**, *254*, 113054. [\[CrossRef\]](#)
29. Li, J.; Gong, Y.; Jiang, C. Spatio-temporal differentiation and policy optimization of ecological well-being in the Yellow River Delta high-efficiency eco-economic zone. *J. Clean. Prod.* **2022**, *339*, 130717. [\[CrossRef\]](#)
30. Zeng, Y.; Cao, Y.; Qiao, X.; Seyler, B.C.; Tang, Y. Air pollution reduction in China: Recent success but great challenge for the future. *Sci. Total Environ.* **2019**, *663*, 329–337. [\[CrossRef\]](#)
31. Usman, M.; Balsalobre-Lorente, D. Environmental concern in the era of industrialization: Can financial development, renewable energy and natural resources alleviate some load? *Energy Policy* **2022**, *162*, 112780. [\[CrossRef\]](#)

32. Shao, M.; Tang, X.; Zhang, Y.; Li, W. City clusters in China: Air and surface water pollution. *Front. Ecol. Environ.* **2006**, *4*, 353–361. [\[CrossRef\]](#)
33. Riti, J.S.; Song, D.; Shu, Y.; Kamah, M. Decoupling CO₂ emission and economic growth in China: Is there consistency in estimation results in analyzing environmental Kuznets curve? *J. Clean. Prod.* **2017**, *166*, 1448–1461. [\[CrossRef\]](#)
34. Wang, Z.; Huang, X.; Wang, N.; Xu, J.; Ding, A. Aerosol-radiation interactions of dust storm deteriorate particle and ozone pollution in East China. *J. Geophys. Res. Atmos.* **2020**, *125*, e2020JD033601. [\[CrossRef\]](#)
35. Sutton, R.T. ESD Ideas: A simple proposal to improve the contribution of IPCC WGI to the assessment and communication of climate change risks. *Earth Syst. Dyn.* **2018**, *9*, 1155–1158. [\[CrossRef\]](#)
36. Dong, F.; Li, J.; Huang, J.; Lu, Y.; Qin, C.; Zhang, X.; Lu, B.; Liu, Y.; Hua, Y. A reverse distribution between synergistic effect and economic development: An analysis from industrial SO₂ decoupling and CO₂ decoupling. *Environ. Impact Assess. Rev.* **2023**, *99*, 107037. [\[CrossRef\]](#)
37. Christensen, M.W.; Gettelman, A.; Cermak, J.; Dagan, G.; Diamond, M.; Douglas, A.; Feingold, G.; Glassmeier, F.; Goren, T.; Grosvenor, D.P. Opportunistic experiments to constrain aerosol effective radiative forcing. *Atmos. Chem. Phys.* **2022**, *22*, 641–674. [\[CrossRef\]](#) [\[PubMed\]](#)
38. Fu, Y.; Gao, H.; Liao, H.; Tian, X. Spatiotemporal variations and uncertainty in crop residue burning emissions over North China plain: Implication for atmospheric CO₂ simulation. *Remote Sens.* **2021**, *13*, 3880. [\[CrossRef\]](#)
39. Song, B.; Gong, J.; Tang, W.; Zeng, G.; Chen, M.; Xu, P.; Shen, M.; Ye, S.; Feng, H.; Zhou, C. Influence of multi-walled carbon nanotubes on the microbial biomass, enzyme activity, and bacterial community structure in 2,4-dichlorophenol-contaminated sediment. *Sci. Total Environ.* **2020**, *713*, 136645. [\[CrossRef\]](#)
40. Cutter, S.L.; Finch, C. Temporal and spatial changes in social vulnerability to natural hazards. *Proc. Natl. Acad. Sci. USA* **2008**, *105*, 2301–2306. [\[CrossRef\]](#)
41. Balogun, A.-L.; Tella, A.; Baloo, L.; Adebisi, N. A review of the inter-correlation of climate change, air pollution and urban sustainability using novel machine learning algorithms and spatial information science. *Urban Clim.* **2021**, *40*, 100989. [\[CrossRef\]](#)
42. Falloon, P.; Betts, R. Climate impacts on European agriculture and water management in the context of adaptation and mitigation—The importance of an integrated approach. *Sci. Total Environ.* **2010**, *408*, 5667–5687. [\[CrossRef\]](#)
43. Gautam, S.; Elizabeth, J.; Gautam, A.S.; Singh, K.; Abhilash, P. Impact assessment of aerosol optical depth on rainfall in Indian rural areas. *Aerosol Sci. Eng.* **2022**, *6*, 186–196. [\[CrossRef\]](#)
44. Persad, G.G. The dependence of aerosols' global and local precipitation impacts on the emitting region. *Atmos. Chem. Phys.* **2023**, *23*, 3435–3452. [\[CrossRef\]](#)
45. Wang, Z.; Xue, L.; Liu, J.; Ding, K.; Lou, S.; Ding, A.; Wang, J.; Huang, X. Roles of atmospheric aerosols in extreme meteorological events: A systematic review. *Curr. Pollut. Rep.* **2022**, *8*, 177–188. [\[CrossRef\]](#)
46. Sillmann, J.; Stjern, C.W.; Myhre, G.; Forster, P.M. Slow and fast responses of mean and extreme precipitation to different forcing in CMIP5 simulations. *Geophys. Res. Lett.* **2017**, *44*, 6383–6390. [\[CrossRef\]](#)
47. Jiang, X.; Li, G.; Fu, W. Government environmental governance, structural adjustment and air quality: A quasi-natural experiment based on the Three-year Action Plan to Win the Blue Sky Defense War. *J. Environ. Manag.* **2021**, *277*, 111470. [\[CrossRef\]](#) [\[PubMed\]](#)
48. Razzaq, A.; Sharif, A.; Aziz, N.; Irfan, M.; Jermisittiparsert, K. Asymmetric link between environmental pollution and COVID-19 in the top ten affected states of US: A novel estimations from quantile-on-quantile approach. *Environ. Res.* **2020**, *191*, 110189. [\[CrossRef\]](#) [\[PubMed\]](#)
49. Dilawar, A.; Chen, B.; Ashraf, A.; Alphonse, K.; Hussain, Y.; Ali, S.; Jinghong, J.; Shafeeque, M.; Boyang, S.; Sun, X. Development of a GIS based hazard, exposure, and vulnerability analyzing method for monitoring drought risk at Karachi, Pakistan. *Geomat. Nat. Hazards Risk* **2022**, *13*, 1700–1720. [\[CrossRef\]](#)
50. Ren, Y.; Liu, J.; Shalamzari, M.J.; Arshad, A.; Liu, S.; Liu, T.; Tao, H. Monitoring Recent Changes in Drought and Wetness in the Source Region of the Yellow River Basin, China. *Water* **2022**, *14*, 861. [\[CrossRef\]](#)
51. Ren, Y.; Liu, J.; Zhang, T.; Shalamzari, M.J.; Arshad, A.; Liu, T.; Willems, P.; Gao, H.; Tao, H.; Wang, T. Identification and Analysis of Heatwave Events Considering Temporal Continuity and Spatial Dynamics. *Remote Sens.* **2023**, *15*, 1369. [\[CrossRef\]](#)
52. Shafeeque, M.; Arshad, A.; Elbeltagi, A.; Sarwar, A.; Pham, Q.B.; Khan, S.N.; Dilawar, A.; Al-Ansari, N. Understanding temporary reduction in atmospheric pollution and its impacts on coastal aquatic system during COVID-19 lockdown: A case study of South Asia. *Geomat. Nat. Hazards Risk* **2021**, *12*, 560–580. [\[CrossRef\]](#)
53. Mumtaz, F.; Arshad, A.; Mirchi, A.; Tariq, A.; Dilawar, A.; Hussain, S.; Shi, S.; Noor, R.; Noor, R.; Daccache, A. Impacts of reduced deposition of atmospheric nitrogen on coastal marine eco-system during substantial shift in human activities in the twenty-first century. *Geomat. Nat. Hazards Risk* **2021**, *12*, 2023–2047. [\[CrossRef\]](#)
54. Rahman, M.M.; Shuo, W.; Zhao, W.; Xu, X.; Zhang, W.; Arshad, A. Investigating the Relationship between Air Pollutants and Meteorological Parameters Using Satellite Data over Bangladesh. *Remote Sens.* **2022**, *14*, 2757. [\[CrossRef\]](#)
55. Mak, H.W.L.; Laughner, J.L.; Fung, J.C.H.; Zhu, Q.; Cohen, R.C. Improved satellite retrieval of tropospheric NO₂ column density via updating of air mass factor (AMF): Case study of Southern China. *Remote Sens.* **2018**, *10*, 1789. [\[CrossRef\]](#)
56. Li, C.; Joiner, J.; Liu, F.; Krotkov, N.A.; Fioletov, V.; McLinden, C. A new machine-learning-based analysis for improving satellite-retrieved atmospheric composition data: OMI SO₂ as an example. *Atmos. Meas. Tech.* **2022**, *15*, 5497–5514. [\[CrossRef\]](#)

57. Wenig, M.O.; Cede, A.; Bucsela, E.; Celarier, E.; Boersma, K.; Veefkind, J.; Brinksma, E.; Gleason, J.; Herman, J. Validation of OMI tropospheric NO₂ column densities using direct-Sun mode Brewer measurements at NASA Goddard Space Flight Center. *J. Geophys. Res. Atmos.* **2008**, *113*. [\[CrossRef\]](#)
58. Duncan, B.N.; Yoshida, Y.; de Foy, B.; Lamsal, L.N.; Streets, D.G.; Lu, Z.; Pickering, K.E.; Krotkov, N.A. The observed response of Ozone Monitoring Instrument (OMI) NO₂ columns to NO_x emission controls on power plants in the United States: 2005–2011. *Atmos. Environ.* **2013**, *81*, 102–111. [\[CrossRef\]](#)
59. Xue, R.; Wang, S.; Li, D.; Zou, Z.; Chan, K.L.; Valks, P.; Saiz-Lopez, A.; Zhou, B. Spatio-temporal variations in NO₂ and SO₂ over Shanghai and Chongming Eco-Island measured by Ozone Monitoring Instrument (OMI) during 2008–2017. *J. Clean. Prod.* **2020**, *258*, 120563. [\[CrossRef\]](#)
60. Zhang, L.; Lee, C.S.; Zhang, R.; Chen, L. Spatial and temporal evaluation of long term trend (2005–2014) of OMI retrieved NO₂ and SO₂ concentrations in Henan Province, China. *Atmos. Environ.* **2017**, *154*, 151–166. [\[CrossRef\]](#)
61. Essou, G.R.; Brissette, F.; Lucas-Picher, P. The use of reanalyses and gridded observations as weather input data for a hydrological model: Comparison of performances of simulated river flows based on the density of weather stations. *J. Hydrometeorol.* **2017**, *18*, 497–513. [\[CrossRef\]](#)
62. Hammer, M.S.; van Donkelaar, A.; Li, C.; Lyapustin, A.; Sayer, A.M.; Hsu, N.C.; Levy, R.C.; Garay, M.J.; Kalashnikova, O.V.; Kahn, R.A. Global estimates and long-term trends of fine particulate matter concentrations (1998–2018). *Environ. Sci. Technol.* **2020**, *54*, 7879–7890. [\[CrossRef\]](#)
63. Van Donkelaar, A.; Martin, R.V.; Brauer, M.; Hsu, N.C.; Kahn, R.A.; Levy, R.C.; Lyapustin, A.; Sayer, A.M.; Winker, D.M. Global estimates of fine particulate matter using a combined geophysical-statistical method with information from satellites, models, and monitors. *Environ. Sci. Technol.* **2016**, *50*, 3762–3772. [\[CrossRef\]](#) [\[PubMed\]](#)
64. Chen, L.; Gao, Y.; Zhu, D.; Yuan, Y.; Liu, Y. Quantifying the scale effect in geospatial big data using semi-variograms. *PLoS ONE* **2019**, *14*, e0225139. [\[CrossRef\]](#) [\[PubMed\]](#)
65. Muñoz-Sabater, J.; Dutra, E.; Agustí-Panareda, A.; Albergel, C.; Arduini, G.; Balsamo, G.; Boussetta, S.; Choulga, M.; Harrigan, S.; Hersbach, H. ERA5-Land: A state-of-the-art global reanalysis dataset for land applications. *Earth Syst. Sci. Data* **2021**, *13*, 4349–4383. [\[CrossRef\]](#)
66. Nazeer, A.; Maskey, S.; Skaugen, T.; McClain, M.E. Simulating the hydrological regime of the snow fed and glacierised Gilgit Basin in the Upper Indus using global precipitation products and a data parsimonious precipitation-runoff model. *Sci. Total Environ.* **2022**, *802*, 149872. [\[CrossRef\]](#)
67. Zhang, H.; Wang, S.; Hao, J.; Wang, X.; Wang, S.; Chai, F.; Li, M. Air pollution and control action in Beijing. *J. Clean. Prod.* **2016**, *112*, 1519–1527. [\[CrossRef\]](#)
68. Chen, R.; De Sherbinin, A.; Ye, C.; Shi, G. China's soil pollution: Farms on the frontline. *Science* **2014**, *344*, 691. [\[CrossRef\]](#)
69. Wang, Z. How Aquatic Chemistry Took Root and Has Flourished in China: Classical Textbooks, a Tale of Two Manganese, and a Dynamic Community. *Environ. Sci. Technol.* **2021**, *55*, 14353–14359. [\[CrossRef\]](#)
70. People's, B.S.C.o.t.a.R.o.C. State Council of the People's Republic of China 2013 Notice of the general office of the state council on issuing the air pollution prevention and control action plan 2013. *Rep. No. Guofa* **2013**, *37*, 2037.
71. Geng, G.; Zheng, Y.; Zhang, Q.; Xue, T.; Zhao, H.; Tong, D.; Zheng, B.; Li, M.; Liu, F.; Hong, C. Drivers of PM_{2.5} air pollution deaths in China 2002–2017. *Nat. Geosci.* **2021**, *14*, 645–650. [\[CrossRef\]](#)
72. Zhong, Q.; Tao, S.; Ma, J.; Liu, J.; Shen, H.; Shen, G.; Guan, D.; Yun, X.; Meng, W.; Yu, X. PM_{2.5} reductions in Chinese cities from 2013 to 2019 remain significant despite the inflating effects of meteorological conditions. *One Earth* **2021**, *4*, 448–458. [\[CrossRef\]](#)
73. Gao, J.; Woodward, A.; Vardoulakis, S.; Kovats, S.; Wilkinson, P.; Li, L.; Xu, L.; Li, J.; Yang, J.; Cao, L. Haze, public health and mitigation measures in China: A review of the current evidence for further policy response. *Sci. Total Environ.* **2017**, *578*, 148–157. [\[CrossRef\]](#) [\[PubMed\]](#)
74. Wang, S.; Hao, J. Air quality management in China: Issues, challenges, and options. *J. Environ. Sci.* **2012**, *24*, 2–13. [\[CrossRef\]](#) [\[PubMed\]](#)
75. Zhang, S.; Li, Y.; Hao, Y.; Zhang, Y. Does public opinion affect air quality? Evidence based on the monthly data of 109 prefecture-level cities in China. *Energy Policy* **2018**, *116*, 299–311. [\[CrossRef\]](#)
76. Chen, L.; Zhu, J.; Liao, H.; Yang, Y.; Yue, X. Meteorological influences on PM_{2.5} and O₃ trends and associated health burden since China's clean air actions. *Sci. Total Environ.* **2020**, *744*, 140837. [\[CrossRef\]](#) [\[PubMed\]](#)
77. Zang, H.; Guo, M.; Wei, Z.; Sun, G. Determination of the optimal tilt angle of solar collectors for different climates of China. *Sustainability* **2016**, *8*, 654. [\[CrossRef\]](#)
78. Porter, S.C. Chinese loess record of monsoon climate during the last glacial–interglacial cycle. *Earth-Sci. Rev.* **2001**, *54*, 115–128. [\[CrossRef\]](#)
79. Krotkov, N.; Lamsal, L.; Marchenko, S.; Celarier, E.; Bucsela, E.; Swartz, W.; Joiner, J. *The OMI Core Team: OMI/Aura NO₂ Total and Tropospheric Column Daily L2 Global Gridded 0.25 Degree × 0.25 Degree V3*; NASA Goddard Space Flight Center, Goddard Earth Sciences Data and Information Services Center (GES DISC): Greenbelt, MD, USA, 2019.
80. Li, C.; Krotkov, N.; Leonard, P. *OMI/Aura Sulfur Dioxide (SO₂) Total Column L3 1 Day Best Pixel in 0.25 Degree x 0.25 Degree V3*; Greenbelt, MD, USA, Goddard Earth Sciences Data and Information Services Center (GES DISC): Greenbelt, MD, USA, 2020.

81. Veefkind, P. *OMI/Aura Ozone (O₃) DOAS Total Column L3 1 Day 0.25 Degree x 0.25 Degree V3*; Goddard Earth Sciences Data and Information Services Center (GES DISC): Greenbelt, MD, USA, 2012.
82. Dilawar, A.; Chen, B.; Arshad, A.; Guo, L.; Ehsan, M.I.; Hussain, Y.; Kayiranga, A.; Measho, S.; Zhang, H.; Wang, F. Towards understanding variability in droughts in response to extreme climate conditions over the different agro-ecological zones of Pakistan. *Sustainability* **2021**, *13*, 6910. [\[CrossRef\]](#)
83. Assamnew, A.D.; Mengistu Tsidu, G. Assessing improvement in the fifth-generation ECMWF atmospheric reanalysis precipitation over East Africa. *Int. J. Climatol.* **2023**, *43*, 17–37. [\[CrossRef\]](#)
84. Lees, E.; Bousquet, O.; Roy, D.; Bellevue, J.L.D. Analysis of diurnal to seasonal variability of Integrated Water Vapour in the South Indian Ocean basin using ground-based GNSS and fifth-generation ECMWF reanalysis (ERA5) data. *Q. J. R. Meteorol. Soc.* **2021**, *147*, 229–248. [\[CrossRef\]](#)
85. Şen, Z. Trend identification simulation and application. *J. Hydrol. Eng.* **2014**, *19*, 635–642. [\[CrossRef\]](#)
86. Dong, Z.; Jia, W.; Sarukkalige, R.; Fu, G.; Meng, Q.; Wang, Q. Innovative trend analysis of air temperature and precipitation in the jinsha river basin, china. *Water* **2020**, *12*, 3293. [\[CrossRef\]](#)
87. Alifujiang, Y.; Abuduwaili, J.; Maihemuti, B.; Emin, B.; Groll, M. Innovative trend analysis of precipitation in the Lake Issyk-Kul Basin, Kyrgyzstan. *Atmosphere* **2020**, *11*, 332. [\[CrossRef\]](#)
88. Şen, Z. *Innovative Trend Methodologies in Science and Engineering*; Springer: Berlin/Heidelberg, Germany, 2017.
89. Wang, Y.; Xu, Y.; Tabari, H.; Wang, J.; Wang, Q.; Song, S.; Hu, Z. Innovative trend analysis of annual and seasonal rainfall in the Yangtze River Delta, eastern China. *Atmos. Res.* **2020**, *231*, 104673. [\[CrossRef\]](#)
90. Şen, Z. Innovative trend analysis methodology. *J. Hydrol. Eng.* **2012**, *17*, 1042–1046. [\[CrossRef\]](#)
91. Şen, Z. Innovative trend significance test and applications. *Theor. Appl. Climatol.* **2017**, *127*, 939–947. [\[CrossRef\]](#)
92. Wu, H.; Qian, H. Innovative trend analysis of annual and seasonal rainfall and extreme values in Shaanxi, China, since the 1950s. *Int. J. Climatol.* **2017**, *37*, 2582–2592. [\[CrossRef\]](#)
93. Kendall, M.G. *Rank Correlation Methods*; Springer: Berlin/Heidelberg, Germany, 1948.
94. Hirsch, R.M.; Slack, J.R. A nonparametric trend test for seasonal data with serial dependence. *Water Resour. Res.* **1984**, *20*, 727–732. [\[CrossRef\]](#)
95. Nakaya, T.; Fotheringham, S.; Charlton, M.; Brunsdon, C. Semiparametric geographically weighted generalised linear modelling in GWR 4.0. In Proceedings of the 10th International Conference on Geocomputation, Sydney, Australia, 30 November–2 December 2009. Available online: http://www.geocomputation.org/2009/PDF/Nakaya_et_al.pdf (accessed on 2 September 2022).
96. Deng, M.; Chen, D.; Zhang, G.; Cheng, H. Policy-driven variations in oxidation potential and source apportionment of PM_{2.5} in Wuhan, central China. *Sci. Total Environ.* **2022**, *853*, 158255. [\[CrossRef\]](#)
97. Yu, Y.; Dai, C.; Wei, Y.; Ren, H.; Zhou, J. Air pollution prevention and control action plan substantially reduced PM_{2.5} concentration in China. *Energy Econ.* **2022**, *113*, 106206. [\[CrossRef\]](#)
98. Li, J. Pollution trends in China from 2000 to 2017: A multi-sensor view from space. *Remote Sens.* **2020**, *12*, 208. [\[CrossRef\]](#)
99. Xu, J.; Lindqvist, H.; Liu, Q.; Wang, K.; Wang, L. Estimating the spatial and temporal variability of the ground-level NO₂ concentration in China during 2005–2019 based on satellite remote sensing. *Atmos. Pollut. Res.* **2021**, *12*, 57–67. [\[CrossRef\]](#)
100. Zou, C.; Wu, L.; Wang, Y.; Sun, S.; Wei, N.; Sun, B.; Ni, J.; He, J.; Zhang, Q.; Peng, J. Evaluating traffic emission control policies based on large-scale and real-time data: A case study in central China. *Sci. Total Environ.* **2023**, *860*, 160435. [\[CrossRef\]](#) [\[PubMed\]](#)
101. Liou, Y.-A.; Vo, T.-H.; Nguyen, K.-A.; Terry, J.P. Air Quality Improvement Following COVID-19 Lockdown Measures and Projected Benefits for Environmental Health. *Remote Sens.* **2023**, *15*, 530. [\[CrossRef\]](#)
102. Zhou, R.; Yan, C.; Yang, Q.; Niu, H.; Liu, J.; Xue, F.; Chen, B.; Zhou, T.; Chen, H.; Liu, J. Characteristics of wintertime carbonaceous aerosols in two typical cities in Beijing-Tianjin-Hebei region, China: Insights from multiyear measurements. *Environ. Res.* **2023**, *216*, 114469. [\[CrossRef\]](#)
103. Yang, F.; Tan, J.; Zhao, Q.; Du, Z.; He, K.; Ma, Y.; Duan, F.; Chen, G. Characteristics of PM 2.5 speciation in representative megacities and across China. *Atmos. Chem. Phys.* **2011**, *11*, 5207–5219. [\[CrossRef\]](#)
104. Cui, H.; Chen, W.; Dai, W.; Liu, H.; Wang, X.; He, K. Source apportionment of PM_{2.5} in Guangzhou combining observation data analysis and chemical transport model simulation. *Atmos. Environ.* **2015**, *116*, 262–271. [\[CrossRef\]](#)
105. Tong, R.; Liu, J.; Wang, W.; Fang, Y. Health effects of PM_{2.5} emissions from on-road vehicles during weekdays and weekends in Beijing, China. *Atmos. Environ.* **2020**, *223*, 117258. [\[CrossRef\]](#)
106. Mak, H.W.L.; Ng, D.C.Y. Spatial and Socio-Classification of Traffic Pollutant Emissions and Associated Mortality Rates in High-Density Hong Kong via Improved Data Analytic Approaches. *Int. J. Environ. Res. Public Health* **2021**, *18*, 6532. [\[CrossRef\]](#)
107. Wu, X.; Wu, Y.; Zhang, S.; Liu, H.; Fu, L.; Hao, J. Assessment of vehicle emission programs in China during 1998–2013: Achievement, challenges and implications. *Environ. Pollut.* **2016**, *214*, 556–567. [\[CrossRef\]](#) [\[PubMed\]](#)
108. Liu, Y.; Wang, T. Worsening urban ozone pollution in China from 2013 to 2017–Part 1: The complex and varying roles of meteorology. *Atmos. Chem. Phys.* **2020**, *20*, 6305–6321. [\[CrossRef\]](#)
109. Liu, Y.; Wang, T. Worsening urban ozone pollution in China from 2013 to 2017–Part 2: The effects of emission changes and implications for multi-pollutant control. *Atmos. Chem. Phys.* **2020**, *20*, 6323–6337. [\[CrossRef\]](#)
110. Sicard, P.; De Marco, A.; Agathokleous, E.; Feng, Z.; Xu, X.; Paoletti, E.; Rodriguez, J.J.D.; Calatayud, V. Amplified ozone pollution in cities during the COVID-19 lockdown. *Sci. Total Environ.* **2020**, *735*, 139542. [\[CrossRef\]](#) [\[PubMed\]](#)

111. Siciliano, B.; Dantas, G.; da Silva, C.M.; Arbilla, G. Increased ozone levels during the COVID-19 lockdown: Analysis for the city of Rio de Janeiro, Brazil. *Sci. Total Environ.* **2020**, 737, 139765. [[CrossRef](#)]
112. XueB, M.B.; Geng, Y. A review on China's pol-lutant emissions reduction assessment. *Ecol. Indica-Tors* **2014**, 38, 272–278.

Disclaimer/Publisher's Note: The statements, opinions and data contained in all publications are solely those of the individual author(s) and contributor(s) and not of MDPI and/or the editor(s). MDPI and/or the editor(s) disclaim responsibility for any injury to people or property resulting from any ideas, methods, instructions or products referred to in the content.